

Deformation of a Half-Space from Anelastic Strain Confined in a Tetrahedral Volume

Sylvain Barbot¹

¹Earth Observatory of Singapore, Nanyang Technological University

Abstract

Deformation in the lithosphere-asthenosphere system can be accommodated by faulting and plastic flow. However, incorporating structural data in models of distributed deformation still represents a challenge. Here, I present solutions for the displacements and stress in a half-space caused by distributed anelastic strain confined in a tetrahedral volume. These solutions form the basis of curvilinear meshes that can adapt to realistic structural settings, such as a mantle wedge corner, a spherical shell around a magma chamber, or an aquifer. I provide computer programs to evaluate them in the cases of anti-plane strain, in-plane strain, and three-dimensional deformation. These tools may prove useful in the modeling of deformation data in tectonics, volcanology, and hydrology.

Introduction

Earth's deformation encompasses physical processes that spread widely across space-time. The deformation of the lithosphere-asthenosphere system is largely accommodated by localized (faulting) and distributed (e.g., plastic flow, multiphase flow) deformation. Because of the urgency of understanding seismic hazards, a large body of work is dedicated to describing brittle deformation (*Chinnery, 1963; Iwasaki and Sato, 1979; Jeyakumaran et al., 1992; Meade, 2007; Nikkhoo and Walter, 2015; Okada, 1985, 1992; Sato and Matsu'ura, 1974; Savage and Hastie, 1966; Steketee, 1958; Wang et al., 2003*). Recently, *Barbot et al. (2017)* described how distributed plastic deformation induces displacement and stress in the surrounding medium, opening the door to low-frequency and time-dependent tomography from deformation data (*Moore et al., 2017; Qiu et al., 2018; Tsang et al., 2016*) and to more comprehensive forward models of deformation in the lithosphere-asthenosphere system that include the mechanical coupling between brittle and viscoelastic deformation (*Barbot, 2018; Lambert and Barbot, 2016*).

Increasingly accurate images of Earth's internal strain and strain-rates require incorporating morphological gradients (e.g., *Barnhart and Lohman, 2010; Dieterich and Richards-Dinger, 2010; Furuya and Yasuda, 2011; Li and Liu, 2016; Marshall et al., 2009; Murray and Langbein, 2006; Qiu et al., 2016; Steer et al., 2014; Walter and Amelung, 2006*). A familiar approach in fault mechanics is to discretize faults in triangular elements, as they can conform to curvilinear surfaces at least to first-order approximation (*Comninou and Dundurs, 1975; Gosling and Willis, 1994; Jeyakumaran et al., 1992; Maerten et al., 2005; Meade, 2007; Nikkhoo and Walter, 2015; Ohtani and Hirahara, 2015; Yoffe, 1960*). It is natural to extend the approach to tetrahedral volumes for distributed anelastic strain to conform volume meshes to structural data. Rectangular and triangular fault elements and cuboidal and tetrahedral volumes can be combined to represent various physical processes of deformation in a realistic geometry. Figure 1 illustrates how different types of fault and volume elements can be combined to represent the kinematics or quasi-dynamics of a regional block of the

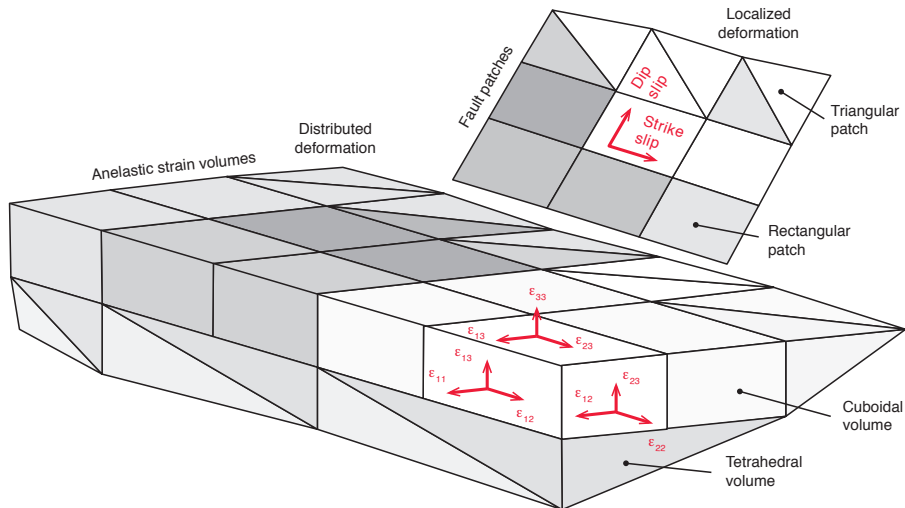


Figure 1: Schematic view of the modeling approach. Localized deformation is discretized with triangular or rectangular boundary elements representing fault slip. Distributed deformation is discretized with tetrahedral or cuboidal volume elements representing plastic deformation. The surrounding elastic material is not meshed but its effect is included in the Green's functions. Curvilinear surfaces and volumes can be approximated with triangular and tetrahedral elements.

lithosphere-asthenosphere system. Fault processes can be represented by triangular or rectangular boundary elements and distributed deformation processes can be discretized with tetrahedral or cuboidal volume elements.

In this paper, I focus on anelastic deformation confined in a tetrahedral volume for three-dimensional problems and triangular surfaces for two-dimensional problems. More complex deformation can be reproduced by a linear combination of these elementary solutions. In the next two sections, I describe the governing equations and derive a simple general expression for the displacement kernels for arbitrary volumes of quasi-static anelastic deformation. Then, I derive the displacement and stress kernels for the cases of anti-plane strain, plane strain, and three-dimensional deformation. In the last section, I derive numerical solutions based on fast Fourier transforms that are more amenable to large-scale problems.

Eigenstrain and equivalent body forces

The deformation of materials can be broadly categorized into elastic and anelastic deformation. Elastic deformation is reversible, implying that the material spontaneously recovers its original configuration when the loads are re-

moved. Until then, the material remains under stress, following the constitutive stress/elastic strain relationship

$$\boldsymbol{\sigma} = \mathbf{C} : \boldsymbol{\epsilon}^e , \quad (1)$$

where $\boldsymbol{\sigma}$ is the Cauchy stress, \mathbf{C} is the elastic moduli tensor, assumed independent of anelastic strain, and $\boldsymbol{\epsilon}^e$ is the elastic strain tensor. Anelastic deformation requires additional work to place the material back into its original configuration and is thermodynamically irreversible. Many deformation processes within the Earth, such as poroelasticity, viscoelasticity, and faulting are anelastic (*Barbot and Fialko, 2010a,b*). Therefore, manipulating the total strain in the medium as the sum of the elastic and anelastic contributions (e.g., *Andrews, 1978*)

$$\boldsymbol{\epsilon} = \boldsymbol{\epsilon}^e + \boldsymbol{\epsilon}^i , \quad (2)$$

where $\boldsymbol{\epsilon}^i$ represents the cumulative anelastic strain, is a useful approximation. In practical applications the anelastic strain or its time derivative is known, either provided by the constitutive behavior of the material under a given stress (e.g., *Barbot, 2018*) or inverted for (e.g., *Qiu et al., 2018*). The conservation of linear momentum at steady state leads to the following governing equation for the total strain

$$\nabla \cdot (\mathbf{C} : \boldsymbol{\epsilon}) + \mathbf{f} = \mathbf{0} , \quad (3)$$

where the anelastic strain has been associated with the equivalent body-force density

$$\mathbf{f} = -\nabla \cdot \mathbf{m} , \quad (4)$$

and the moment density $\mathbf{m} = \mathbf{C} : \boldsymbol{\epsilon}^i$. The total displacement $\mathbf{u}(\mathbf{x})$ due to anelastic strain and the elastic response of the medium can be obtained by solving the momentum equation (3). The total strain follows as

$$\boldsymbol{\epsilon} = \frac{1}{2} (\nabla \mathbf{u} + \nabla \mathbf{u}^t) , \quad (5)$$

where $\nabla \mathbf{u}^t$ is the transpose of the displacement gradient. Finally, the stress field is derived by removing the anelastic strain contribution combining (1) and (2), as follows

$$\boldsymbol{\sigma} = \mathbf{C} : (\boldsymbol{\epsilon} - \boldsymbol{\epsilon}^i) . \quad (6)$$

Navier's equation (3) applies to quasi-static deformation due to an arbitrary distribution of anelastic strain under the infinitesimal strain approximation and is valid as long as plastic deformation does not affect the elastic moduli in the medium and inertia can be ignored. As a numerical approximation, I assume piecewise uniform anelastic strain distributions, called transformation strain, within closed volumes Ω_k , so that the displacement can be written as

$$\mathbf{u}(\mathbf{x}) \approx \sum_k \int_{\Omega_k} \mathbf{G}(\mathbf{x}, \mathbf{y}) \cdot \mathbf{f}_k(\mathbf{y}) \, d\mathbf{y} , \quad (7)$$

where \mathbf{f}_k is the equivalent body force for a homogeneous anelastic strain in the domain Ω_k and $\mathbf{G}(\mathbf{x};\mathbf{y})$ are the Green's functions for a point force. The displacement kernels in (7) form the basic ingredients for forward (*Barbot, 2018; Lambert and Barbot, 2016*) and inverse (*Moore et al., 2017; Qiu et al., 2018; Tsang et al., 2016*) modeling of deformation. The closed-form analytic solution of (7) for cuboid volumes of transformation strain is provided by *Barbot et al. (2017)*. To facilitate the meshing of curvilinear surfaces and volumes, I now make the assumption that the transformation strain is confined in a tetrahedral volume.

Displacement kernels

To develop the solution for the displacement kernel (I drop the subscript k for the sake of clarity)

$$\mathbf{u}(\mathbf{x}) = \int_{\Omega} \mathbf{G}(\mathbf{x}, \mathbf{y}) \cdot \mathbf{f}(\mathbf{y}) \, d\mathbf{y} \quad (8)$$

associated with a uniform transformation strain confined within a elementary volume Ω , I write the moment density as

$$\mathbf{m}(\mathbf{x}) = \Phi(\mathbf{x}) \mathbf{m}_0 \, , \quad (9)$$

where $\Phi(\mathbf{x})$ is a single-variate function that represents the location of the transformation strain,

$$\Phi(\mathbf{x}) = \begin{cases} 1 & \text{if } \mathbf{x} \in \Omega, \\ 0 & \text{otherwise} \, , \end{cases} \quad (10)$$

and \mathbf{m}_0 is a constant tensor. With this definition, the equivalent body force becomes

$$\mathbf{f} = -\mathbf{m}_0 \cdot \nabla \Phi \, . \quad (11)$$

As $\Phi(\mathbf{x})$ is uniform within Ω , I can write

$$\nabla \Phi = \begin{cases} -\mathbf{n} & \text{if } \mathbf{x} \in \partial\Omega \\ 0 & \text{otherwise,} \end{cases} \quad (12)$$

where \mathbf{n} is the outward-pointing unit normal vector to Ω . Combining (8), (11), and (12), the displacement kernel simplifies to the surface integral

$$\mathbf{u}(\mathbf{x}) = \mathbf{m}_0 \cdot \int_{\partial\Omega} \mathbf{G}(\mathbf{x}, \mathbf{y}) \cdot \mathbf{n}(\mathbf{y}) \, d\mathbf{y} \, . \quad (13)$$

The stress can be obtained by differentiation of the Green's function $\mathbf{G}(\mathbf{x}, \mathbf{y})$ itself or of the resulting displacement field, following (5) and (6). Equation (13) represents a convenient framework to evaluate the deformation due to transformation strain confined in volumes of arbitrary shape as the integral equation simplifies to a path integral in two dimensions or to a surface integral in three

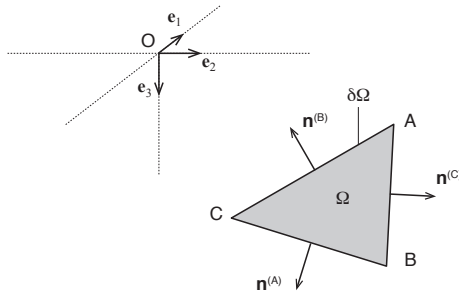


Figure 2: Deformation of a half-space in anti-plane strain due to anelastic strain confined in a triangular element ABC. The vertices A, B, and C have the coordinates \mathbf{x}^A , \mathbf{x}^B , and \mathbf{x}^C , respectively. The normal vectors are pointing outwards, such that $\mathbf{n}^{(C)} \cdot (\mathbf{x}_C - \mathbf{x}_A) \leq 0$ and $\mathbf{n}^{(C)} \cdot (\mathbf{x}_C - \mathbf{x}_B) \leq 0$.

dimension, whereas the form (8) requires a surface integral in two dimensions and a volume integral in three dimensions. In the next sections, I develop solutions for these kernels for triangular surfaces in the cases of anti-plane strain and plane strain and for tetrahedral volumes in the case of three-dimensional deformation. The solution for more complex shapes can be obtained by superposition using the approximation (7).

Distributed deformation of triangular shear zones in anti-plane strain

Two-dimensional models of stress evolution may capture the main features of a mechanical setting (*Savage, 1983; Savage and Prescott, 1978; Thatcher and Rundle, 1979*) and their reduced complexity is more amenable to sensitivity analyses (*Daout et al., 2016a,b; Muto et al., 2016*). The anti-plane strain approximation is relevant to transform plate boundaries (e.g., *Barbot et al., 2008; Erickson et al., 2017; Lambert and Barbot, 2016; Lindsey et al., 2014; Nur and Israel, 1980; Nur and Mavko, 1974*) and curvilinear elements may represent shear zones (e.g., *Takeuchi and Fialko, 2013*) or lower-crustal flow within a realistic stratigraphy.

Problem statement

Consider the elastic deformation in a half-space of rigidity μ in a situation of anti-plane strain caused by distributed anelastic strain confined in an elementary triangular area. In the case of anti-plane strain we have $u_{i,1} = 0$ for $i = 1, 2, 3$ and $u_2 = u_3 = 0$. The transformation strain is confined in a triangular area delimited by three points A, B, and C (Figure 2). The surface is subjected to two independent transformation strain components ϵ_{12}^i and ϵ_{13}^i associated with

the moment density $m_{12} = 2\mu\epsilon_{12}^i$ and $m_{13} = 2\mu\epsilon_{13}^i$. Using (13), the deformation simplifies to the nontrivial component

$$u_1(x_2, x_3) = \int_{\partial\Omega} G_{11}(x_2, x_3, y_2, y_3) (m_{12}n_2 + m_{13}n_3) dy_2 dy_3 , \quad (14)$$

where the Green's function for a line force centered at (y_2, y_3) is obtained by solving Poisson's equation with a Neumann boundary condition and is given by

$$G_{11}(x_2, x_3) = -\frac{1}{4\pi\mu} \left[\ln((x_2 - y_2)^2 + (x_3 - y_3)^2) + \ln((x_2 - y_2)^2 + (x_3 + y_3)^2) \right]. \quad (15)$$

The outward normal vector is different on each side, so we can write

$$\begin{aligned} u_1(x_2, x_3) &= \left(m_{12}n_2^{(C)} + m_{13}n_3^{(C)} \right) \int_{AB} G_{11}(x_2, x_3, y_2, y_3) dy_2 dy_3 \\ &+ \left(m_{12}n_2^{(A)} + m_{13}n_3^{(A)} \right) \int_{BC} G_{11}(x_2, x_3, y_2, y_3) dy_2 dy_3 \\ &+ \left(m_{12}n_2^{(B)} + m_{13}n_3^{(B)} \right) \int_{AC} G_{11}(x_2, x_3, y_2, y_3) dy_2 dy_3 , \end{aligned} \quad (16)$$

where $\mathbf{n}^{(A)}$, $\mathbf{n}^{(B)}$, and $\mathbf{n}^{(C)}$ are the unit normal vectors to the sides BC, AC, and AB, respectively.

Analytic solution

The line integrals (16) are path independent and only depend on the coordinates of the end-points. For any end point A and B, the closed-form solutions can be found using

$$\begin{aligned} \int_{AB} G_{11}(x_2, x_3, y_2, y_3) dy_2 dy_3 &= \Gamma(\mathbf{x}^B) - \Gamma(\mathbf{x}^A) \\ &+ \Gamma(\mathbf{x}^{B'}) - \Gamma(\mathbf{x}^{A'}) , \end{aligned} \quad (17)$$

where \mathbf{x}^A and \mathbf{x}^B are the coordinates of points A and B (Figure 3), A' and B' are the images of points A and B about the surface, and $\Gamma(\mathbf{r})$ is given by

$$\begin{aligned} \Gamma(\mathbf{r}) &= \frac{1}{8\pi} \mathbf{a} \cdot (\mathbf{x} - \mathbf{r}) \ln((\mathbf{x} - \mathbf{r}) \cdot (\mathbf{x} - \mathbf{r})) \\ &+ \frac{1}{4\pi} \mathbf{n} \cdot (\mathbf{x} - \mathbf{r}) \arctan \left[\frac{\mathbf{a} \cdot (\mathbf{x} - \mathbf{r})}{\mathbf{n} \cdot (\mathbf{x} - \mathbf{r})} \right] , \end{aligned} \quad (18)$$

with the unit vector \mathbf{a} aligned with the segment AB and \mathbf{n} a unit vector normal to the segment AB, such that $\mathbf{n} \cdot \mathbf{a} = 0$, and where I have removed the terms that cancel out upon integration over a closed path. The solution to (16) is found by evaluating (17) once for each segments and multiplying the result by

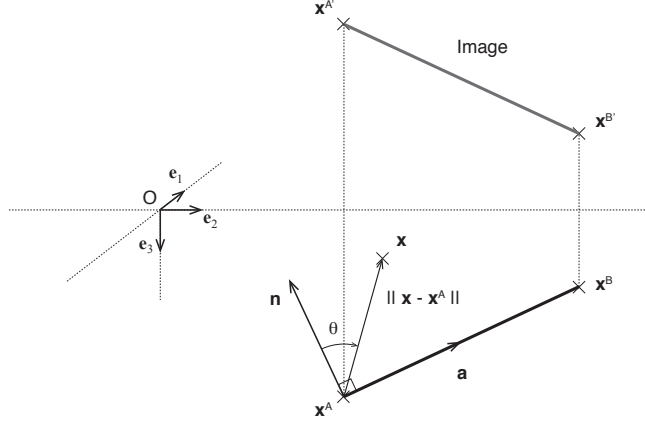


Figure 3: The line integration of the Green's function G_{11} along the segment AB only depend on the coordinates of the end-points \mathbf{x}^A and \mathbf{x}^B . The unit vector \mathbf{a} is parallel to AB and the unit normal vector \mathbf{v} is perpendicular to AB. The image points A' and B' are defined to satisfy the free-surface boundary condition. The local angle is given by $\tan \theta = \mathbf{a} \cdot (\mathbf{x} - \mathbf{r}) / \mathbf{n} \cdot (\mathbf{x} - \mathbf{r})$.

the respective tractions. The displacement gradient is obtained in a similar way using

$$\begin{aligned} \nabla \Gamma(\mathbf{r}) = & \frac{1}{8\pi} \mathbf{a} \ln ((\mathbf{x} - \mathbf{r}) \cdot (\mathbf{x} - \mathbf{r})) \\ & + \frac{1}{4\pi} \mathbf{n} \arctan \left[\frac{\mathbf{a} \cdot (\mathbf{x} - \mathbf{r})}{\mathbf{n} \cdot (\mathbf{x} - \mathbf{r})} \right], \end{aligned} \quad (19)$$

where I have again removed the terms that cancel out upon integration over a closed path. The expressions (18) and (19) are only singular at the end-points A and B.

Semi-analytic solution with the double-exponential and the Gauss-Legendre quadratures

I obtain the solution semi-analytically by solving the line integrals using high-precision numerical quadratures. The Gauss-Legendre quadrature (*Abramowitz and Stegun, 1972; Golub and Welsch, 1969*) provides accurate solutions away from singular points. The double-exponential quadrature (*Haber, 1977*) is more robust to the presence of singularities. To proceed, I consider the line integral

$$I(x_2, x_3) = \int_{AB} G_{11}(x_2, x_3; y_2, y_3) dy_2 dy_3, \quad (20)$$

which I write as a parameterized line integral and in the canonical form of the double-exponential or the Gauss-Legendre quadrature, i.e., within the bounds

of integration -1 and 1 , to get

$$I(x_2, x_3) = \frac{R}{2} \int_{-1}^1 G_{11}(x_2, x_3; y_2(t), y_3(t)) dt, \quad (21)$$

where R is the length of segment AB, t is a dummy variable of integration, and

$$\begin{aligned} y_2(t) &= \frac{x_2^A + x_2^B}{2} + t \frac{x_2^B - x_2^A}{2}, \\ y_3(t) &= \frac{x_3^A + x_3^B}{2} + t \frac{x_3^B - x_3^A}{2}. \end{aligned} \quad (22)$$

The displacement field for a combination of horizontal and vertical shear strain is shown in Figure 4. The numerical solution with the double-exponential quadrature agrees with the analytic solution (17) within double-precision floating-point accuracy (about twelve digits) but takes about 50 times longer to evaluate. The Gauss-Legendre quadrature with just 15 integration points provides high precision in the far-field and can be evaluated almost as fast as the analytic solution. Therefore, switching from the double-exponential to the Gauss-Legendre method when the distance from the circumcenter exceeds 1.75 times the circumradius provides optimal performance without sacrificing accuracy. Two triangles can be combined to form a rectangle. In this case the analytic and semi-analytic solutions agree with the closed-form solution of *Barbot et al.* (2017).

Stress and strain

The stress field can be obtained using (6). For a triangular region with vertices A, B, and C as in Figure 2, the location of the transformation strain is given by

$$\begin{aligned} \Phi(\mathbf{x}) &= H \left[\left(\frac{\mathbf{x}^A + \mathbf{x}^B}{2} - \mathbf{x} \right) \cdot \mathbf{n}^{(C)} \right] \\ &\quad \times H \left[\left(\frac{\mathbf{x}^B + \mathbf{x}^C}{2} - \mathbf{x} \right) \cdot \mathbf{n}^{(A)} \right] \\ &\quad \times H \left[\left(\frac{\mathbf{x}^C + \mathbf{x}^A}{2} - \mathbf{x} \right) \cdot \mathbf{n}^{(B)} \right], \end{aligned} \quad (23)$$

where $H(x)$ is the Heaviside function. An example of the spatial distribution of the shear stress around a triangular strain volume is shown in Figure 5. When two triangles are combined to form a rectangle, it creates the stress field derived by *Barbot et al.* (2017). The semi-analytic solution agrees with the analytic expression based on (19) to double-precision floating point accuracy and takes a similar time to evaluate. This indicates that combining the double-exponential and the Gauss-Legendre quadratures is a viable approach when a closed-form solution is otherwise unavailable.

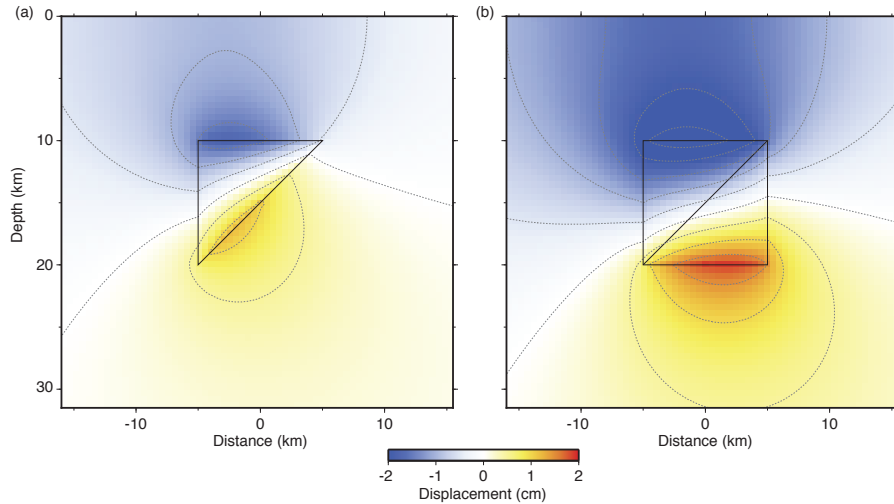


Figure 4: Displacement field in anti-plane strain due to anelastic strain confined in triangular elements (triangles). A) A single triangular element and B) two triangle elements forming a rectangle. The strain volumes are subjected to the transformation strain $\epsilon_{12} = 10^{-6}$ and $\epsilon_{13} = 4 \times 10^{-6}$. The contours (dashed lines) are every 5 mm.

Distributed deformation of triangular strain regions in plane strain

The dynamics of the lithosphere-asthenosphere system around subduction zones, normal faults, and spreading centers may be investigated under the plane strain approximation (Barbot, 2018; Biemiller and Lavier, 2017; Cohen, 1996; Dinther et al., 2013; Goswami and Barbot, 2018; Govers et al., 2017; Hirahara, 2002; Liu and Rice, 2005; Muto et al., 2013; Romanet et al., 2018; Sato and Matsu'ura, 1974; Savage, 1998). In particular, Glas (1991) derived the closed expression for the displacement and stress due to a cuboidal inclusion aligned with the free surface and Barbot et al. (2017) expanded the results for a rotated cuboidal source. In this section, I develop closed-form analytic and semi-analytical solutions for triangular elements of arbitrary orientation to conform with curvilinear meshes. This type of element may prove useful to capture the geometry of the mantle wedge corner, of shear zones below volcanic arcs, or weak regions surrounding dykes and sills.

Problem statement

I consider the elastic deformation in plane strain caused by distributed anelastic strain in an elementary triangular area (Figure 2). In plane strain, we have

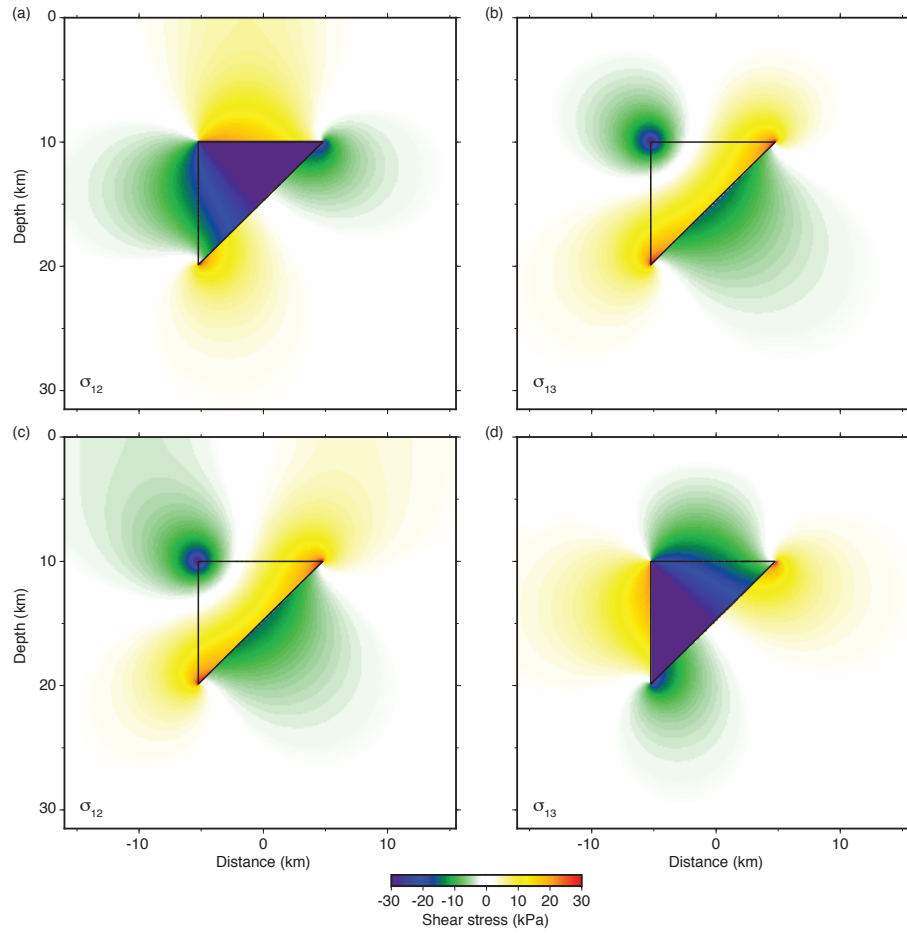


Figure 5: Stress field in anti-plane strain due to anelastic strain confined in triangular elements (triangles). a, c) Horizontal shear stress σ_{12} and b, d) Vertical shear stress σ_{13} . The strain volumes in the left panel are subjected to the transformation strain $\epsilon_{12} = 10^{-6}$. In the right panel, to $\epsilon_{13} = 10^{-6}$.

$u_{1,i} = 0$ for $i = 1, 2, 3$, and $u_1 = 0$. I consider a triangular area delineated by the vertices A , B , and C and subjected to the transformation strain components ϵ_{22}^i , ϵ_{23}^i , ϵ_{32}^i and ϵ_{33}^i , with $\epsilon_{23}^i = \epsilon_{32}^i$. Using (13) again, the deformation simplifies to the nontrivial components

$$\begin{aligned} u_2(x_2, x_3) &= \int_{\partial\Omega} G_{22}(x_2, x_3, y_2, y_3) (m_{22}n_2 + m_{23}n_3) \\ &\quad + G_{32}(x_2, x_3, y_2, y_3) (m_{32}n_2 + m_{33}n_3) \, dy_2 \, dy_3 \\ u_3(x_2, x_3) &= \int_{\partial\Omega} G_{23}(x_2, x_3, y_2, y_3) (m_{22}n_2 + m_{23}n_3) \\ &\quad + G_{33}(x_2, x_3, y_2, y_3) (m_{23}n_2 + m_{33}n_3) \, dy_2 \, dy_3 , \end{aligned} \quad (24)$$

where G_{22} and G_{23} represent the displacements at (x_2, x_3) induced by a line force in the \mathbf{e}_2 direction centered at (y_2, y_3) and G_{32} and G_{33} represent the displacements induced by a line force in the \mathbf{e}_3 direction. They are given by (*Dundurs*, 1962; *Melan*, 1932; *Segall*, 2010)

$$\begin{aligned} G_{22} &= \frac{-1}{2\pi\mu(1-\nu)} \left[\frac{3-4\nu}{4} \ln r_1 + \frac{8\nu^2-12\nu+5}{4} \ln r_2 + \frac{(x_3-y_3)^2}{4r_1^2} \right. \\ &\quad \left. + \frac{(3-4\nu)(x_3+y_3)^2 + 2y_3(x_3+y_3) - 2y_3^2}{4r_2^2} - \frac{y_3x_3(x_3+y_3)^2}{r_2^4} \right] \\ G_{23} &= \frac{1}{2\pi\mu(1-\nu)} \left[(1-2\nu)(1-\nu) \tan^{-1} \frac{x_2-y_2}{x_3+y_3} + \frac{(x_3-y_3)(x_2-y_2)}{4r_1^2} \right. \\ &\quad \left. + (3-4\nu) \frac{(x_3-y_3)(x_2-y_2)}{4r_2^2} - \frac{y_3x_3(x_2-y_2)(x_3+y_3)}{r_2^4} \right] , \\ G_{32} &= \frac{1}{2\pi\mu(1-\nu)} \left[-(1-2\nu)(1-\nu) \tan^{-1} \frac{x_2-y_2}{x_3+y_3} + \frac{(x_3-y_3)(x_2-y_2)}{4r_1^2} \right. \\ &\quad \left. + (3-4\nu) \frac{(x_3-y_3)(x_2-y_2)}{4r_2^2} + \frac{y_3x_3(x_2-y_2)(x_3+y_3)}{r_2^4} \right] \\ G_{33} &= \frac{1}{2\pi\mu(1-\nu)} \left[-\frac{3-4\nu}{4} \ln r_1 - \frac{8\nu^2-12\nu+5}{4} \ln r_2 \right. \\ &\quad \left. - \frac{(x_2-y_2)^2}{4r_1^2} + \frac{2y_3x_3 - (3-4\nu)(x_2-y_2)^2}{4r_2^2} - \frac{y_3x_3(x_2-y_2)^2}{r_2^4} \right] , \end{aligned} \quad (25)$$

with the radii

$$\begin{aligned} r_1^2 &= (x_2-y_2)^2 + (x_3-y_3)^2 \\ r_2^2 &= (x_2-y_2)^2 + (x_3+y_3)^2 . \end{aligned} \quad (26)$$

Breaking down the path integral along the three triangle segments, it becomes

$$\begin{aligned}
u_2(x_2, x_3) = & \left(m_{22}n_2^{(C)} + m_{23}n_3^{(C)} \right) \int_{AB} G_{22}(x_2, x_3; y_2, y_3) \, dy_2 \, dy_3 \\
& + \left(m_{32}n_2^{(C)} + m_{33}n_3^{(C)} \right) \int_{AB} G_{32}(x_2, x_3; y_2, y_3) \, dy_2 \, dy_3 \\
& + \left(m_{22}n_2^{(A)} + m_{23}n_3^{(A)} \right) \int_{BC} G_{22}(x_2, x_3; y_2, y_3) \, dy_2 \, dy_3 \\
& + \left(m_{32}n_2^{(A)} + m_{33}n_3^{(A)} \right) \int_{BC} G_{32}(x_2, x_3; y_2, y_3) \, dy_2 \, dy_3 \\
& + \left(m_{22}n_2^{(B)} + m_{23}n_3^{(B)} \right) \int_{AC} G_{22}(x_2, x_3; y_2, y_3) \, dy_2 \, dy_3 \\
& + \left(m_{32}n_2^{(B)} + m_{33}n_3^{(B)} \right) \int_{AC} G_{32}(x_2, x_3; y_2, y_3) \, dy_2 \, dy_3 ,
\end{aligned} \tag{27}$$

and

$$\begin{aligned}
u_3(x_2, x_3) = & \left(m_{22}n_2^{(C)} + m_{23}n_3^{(C)} \right) \int_{AB} G_{23}(x_2, x_3; y_2, y_3) \, dy_2 \, dy_3 \\
& + \left(m_{32}n_2^{(C)} + m_{33}n_3^{(C)} \right) \int_{AB} G_{33}(x_2, x_3; y_2, y_3) \, dy_2 \, dy_3 \\
& + \left(m_{22}n_2^{(A)} + m_{23}n_3^{(A)} \right) \int_{BC} G_{23}(x_2, x_3; y_2, y_3) \, dy_2 \, dy_3 \\
& + \left(m_{32}n_2^{(A)} + m_{33}n_3^{(A)} \right) \int_{BC} G_{33}(x_2, x_3; y_2, y_3) \, dy_2 \, dy_3 \\
& + \left(m_{22}n_2^{(B)} + m_{23}n_3^{(B)} \right) \int_{AC} G_{23}(x_2, x_3; y_2, y_3) \, dy_2 \, dy_3 \\
& + \left(m_{32}n_2^{(B)} + m_{33}n_3^{(B)} \right) \int_{AC} G_{33}(x_2, x_3; y_2, y_3) \, dy_2 \, dy_3 ,
\end{aligned} \tag{28}$$

where $\mathbf{n}^{(A)}$, $\mathbf{n}^{(B)}$, and $\mathbf{n}^{(C)}$ are the unit normal vectors to the sides BC, AC, and AB, respectively.

Analytic and semi-analytic solutions

The displacement field can be evaluated analytically or using a numerical quadrature using the path integral of the form (21). The closed-form expressions for the line integrals

$$U_{ij} = \int_{AB} G_{ij}(x_2, x_3; y_2, y_3) \, dy_2 \, dy_3 , \tag{29}$$

for the plane-strain Green's functions (25) and $i = 2, 3$ are provided in Appendix A. Examples of displacement fields occasioned by distributed anelastic strain confined in the triangle surface ABC are given in Figure 6. In Figure 7, I show how triangles can be combined to approximate a disk in dilatation. I

have checked that combining two triangles to form a rectangle conforms to the analytic solution of *Barbot et al. (2017)* and that the numerical integration with the double-exponential and the Gauss-Legendre quadratures agrees with the closed-form solution of (29) up to double-precision floating point accuracy for all combinations of sources and displacement components.

Stress and strain

The strain can be obtained by differencing the displacement field analytically or with a finite-difference approximation. An alternative is to directly integrate the Green's functions for the displacement gradient, given below

$$\begin{aligned}
G_{22,2} &= -\frac{x_2 - y_2}{2\pi G(1 - \nu)} \left[\frac{3 - 4\nu}{4r_1^2} + \frac{8\nu^2 - 12\nu + 5}{4r_2^2} - \frac{(x_3 - y_3)^2}{2r_1^4} \right. \\
&\quad \left. - \frac{(3 - 4\nu)(x_3 + y_3)^2 + 2y_3(x_3 + y_3) - 2y_3^2}{2r_2^4} \right. \\
&\quad \left. + \frac{4y_3x_3(x_3 + y_3)^2}{r_2^6} \right] \\
G_{22,3} &= -\frac{1}{2\pi G(1 - \nu)} \left[\frac{(3 - 4\nu)(x_3 - y_3)}{4r_1^2} + \frac{(8\nu^2 - 12\nu + 5)(x_3 + y_3)}{4r_2^2} \right. \\
&\quad + \frac{x_3 - y_3}{2r_1^2} - \frac{(x_3 - y_3)^3}{2r_1^4} + \frac{(3 - 4\nu)(x_3 + y_3) + y_3}{2r_2^2} \\
&\quad - (x_3 + y_3) \frac{(3 - 4\nu)(x_3 + y_3)^2 + 2y_3(x_3 + y_3) - 2y_3^2}{2r_2^4} \\
&\quad - \frac{y_3(x_3 + y_3)^2}{r_2^4} - 2 \frac{y_3x_3(x_3 + y_3)}{r_2^4} \\
&\quad \left. + 4 \frac{x_3y_3(x_3 + y_3)^3}{r_2^6} \right]
\end{aligned} \tag{30}$$

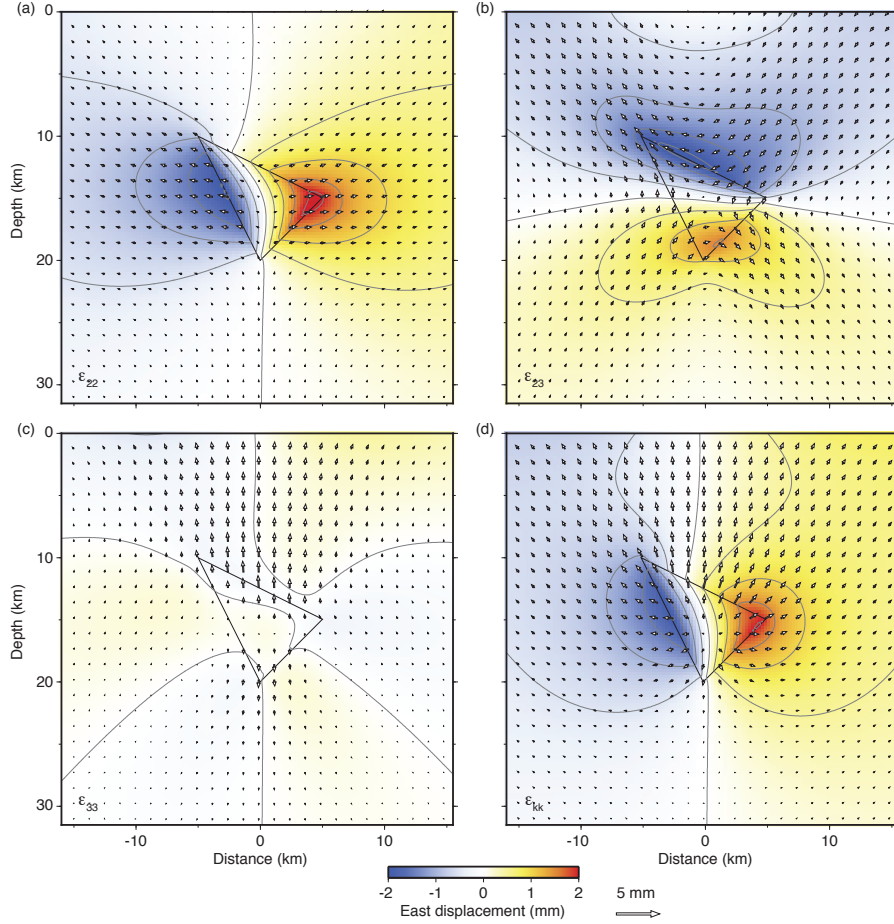


Figure 6: Displacement field in plane strain strain due to anelastic strain confined in triangular elements (triangles). The horizontal displacement is shown by the arrows and the color indicates the horizontal component u_2 . The displacement fields are due to a) horizontal uniaxial extension ($\epsilon_{22} = 10^{-6}$), b) pure shear ($\epsilon_{23} = 10^{-6}$), c) vertical uniaxial extension ($\epsilon_{33} = 10^{-6}$), and d) isotropic extension ($\epsilon_{22} = \epsilon_{33} = 10^{-6}$). The contours (dashed lines) are every 0.5 mm.

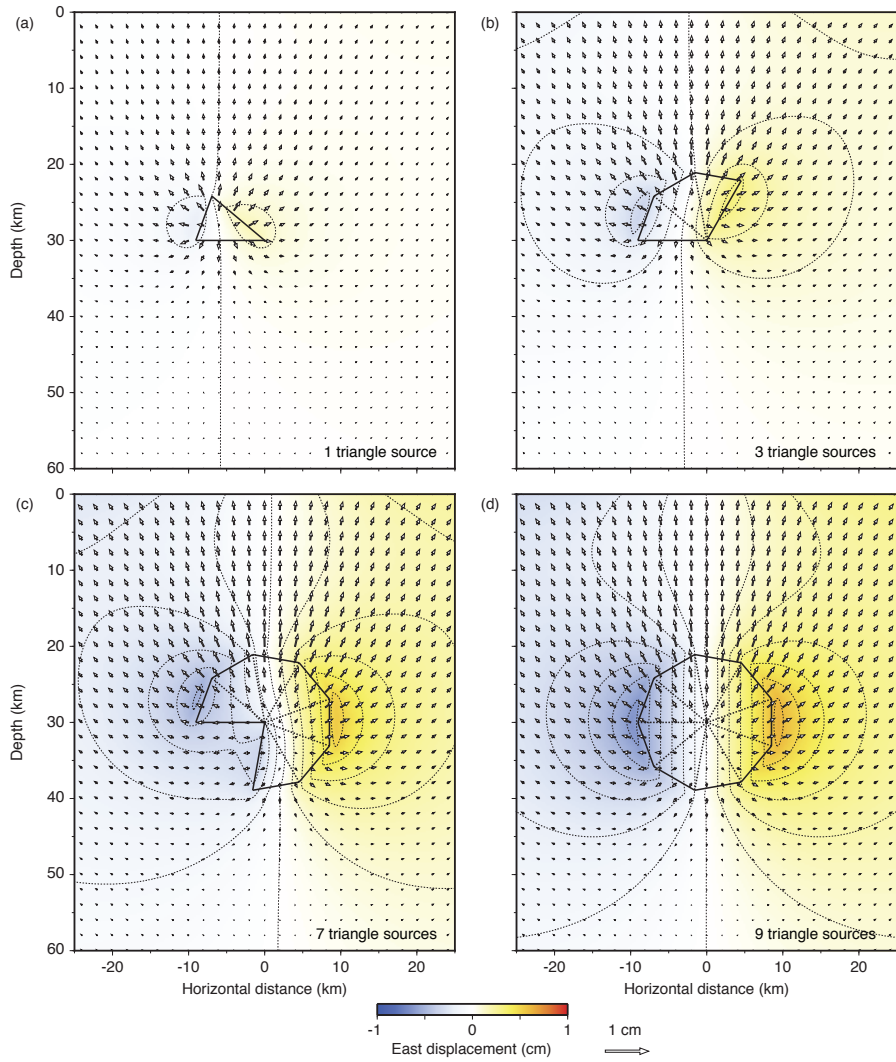


Figure 7: Approximation of the displacement field for a dilating disk by combining 9 triangular sources. The triangles are formed by joining points around the surrounding circle with the center, here at 30 km depth. The background shows the amplitude of the horizontal displacement. The line integrals of the shared segments of adjacent triangles (dashed segments) cancel out, leading to the outwards segments of the combined volume having a non-trivial contribution. a) Displacement field due to an elementary triangle of dilatation. b) Cumulative displacement field due to three triangles. c) Case for 7 triangles. d) Displacement field approximated with 9 triangular sources. The dashed contours are every 1 mm of horizontal displacement.

$$\begin{aligned}
G_{23,2} &= \frac{1}{2\pi G(1-\nu)} \left[(1-2\nu)(1-\nu) \frac{x_3+y_3}{r_2^2} + \frac{x_3-y_3}{4r_1^2} \right. \\
&\quad - \frac{(x_3-y_3)(x_2-y_2)^2}{2r_1^4} + (3-4\nu) \frac{x_3-y_3}{4r_2^2} \\
&\quad - (3-4\nu) \frac{(x_3-y_3)(x_2-y_2)^2}{2r_2^4} - \frac{y_3 x_3 (x_3+y_3)}{r_2^4} \\
&\quad \left. + 4 \frac{y_3 x_3 (x_2-y_2)^2 (x_3+y_3)}{r_2^6} \right], \\
G_{23,3} &= \frac{x_2-y_2}{2\pi G(1-\nu)} \left[- (1-2\nu)(1-\nu) \frac{1}{r_2^2} + \frac{1}{4r_1^2} \right. \\
&\quad - \frac{(x_3-y_3)^2}{2r_1^4} + \frac{(3-4\nu)}{4r_2^2} \\
&\quad - \frac{(3-4\nu)(x_3-y_3)(x_3+y_3)}{2r_2^4} \\
&\quad - \frac{y_3(x_3+y_3)}{r_2^4} - \frac{y_3 x_3}{r_2^4} \\
&\quad \left. + 4 \frac{y_3 x_3 (x_3+y_3)^2}{r_2^6} \right], \tag{31} \\
G_{32,2} &= \frac{1}{2\pi G(1-\nu)} \left[- (1-2\nu)(1-\nu) \frac{x_3+y_3}{r_2^2} + \frac{x_3-y_3}{4r_1^2} \right. \\
&\quad - \frac{(x_3-y_3)(x_2-y_2)^2}{2r_1^4} + \frac{(3-4\nu)(x_3-y_3)}{4r_2^2} \\
&\quad - \frac{(3-4\nu)(x_3-y_3)(x_2-y_2)^2}{2r_2^4} + \frac{y_3 x_3 (x_3+y_3)}{r_2^4} \\
&\quad \left. - 4 \frac{y_3 x_3 (x_2-y_2)^2 (x_3+y_3)}{r_2^6} \right], \\
G_{32,3} &= \frac{x_2-y_2}{2\pi G(1-\nu)} \left[(1-2\nu)(1-\nu) \frac{1}{r_2^2} + \frac{1}{4r_1^2} \right. \\
&\quad - \frac{(x_3-y_3)^2}{2r_1^4} + (3-4\nu) \frac{1}{4r_2^2} \\
&\quad - (3-4\nu) \frac{(x_3-y_3)(x_3+y_3)}{2r_2^4} \\
&\quad + \frac{y_3(x_3+y_3)}{r_2^4} + \frac{y_3 x_3}{r_2^4} \\
&\quad \left. - 4 \frac{y_3 x_3 (x_3+y_3)^2}{r_2^6} \right], \tag{32}
\end{aligned}$$

$$\begin{aligned}
G_{33,2} = & -\frac{x_2 - y_2}{2\pi G(1 - \nu)} \left[(3 - 4\nu) \frac{1}{4r_1^2} + (8\nu^2 - 12\nu + 5) \frac{1}{4r_2^2} \right. \\
& + \frac{1}{2r_1^2} - \frac{(x_2 - y_2)^2}{2r_1^4} \\
& + (3 - 4\nu) \frac{1}{2r_2^2} \\
& + \frac{2y_2x_3 - (3 - 4\nu)(x_2 - y_2)^2}{2r_2^4} \\
& \left. + 2 \frac{y_3x_3}{r_2^4} - 4 \frac{x_3y_3(x_2 - y_2)^2}{r_2^6} \right], \tag{33} \\
G_{33,3} = & \frac{1}{2\pi G(1 - \nu)} \left[-\frac{(3 - 4\nu)(x_3 - y_3)}{4r_1^2} - \frac{(8\nu^2 - 12\nu + 5)(x_3 + y_3)}{4r_2^2} \right. \\
& + \frac{(x_2 - y_2)^2(x_3 - y_3)}{2r_1^4} + \frac{y_2}{2r_2^2} \\
& - (x_3 + y_3) \frac{2y_2x_3 - (3 - 4\nu)(x_2 - y_2)^2}{2r_2^4} \\
& \left. - \frac{y_3(x_2 - y_2)^2}{r_2^4} + 4 \frac{x_3y_3(x_2 - y_2)^2(x_3 + y_3)}{r_2^6} \right],
\end{aligned}$$

where the comma in expressions like $G_{ij,k}$ indicates differentiation of the tensor component G_{ij} with respect to x_k . Importantly, in all the terms forming the Green's function (25) and their derivatives (30-33), the only singular point is at $\mathbf{x} = \mathbf{y}$. This guarantees that the displacement and stress solutions based on numerical integration of the Green's function will be numerically stable at any point away from the source. This property provides an appealing reason to resort to numerical quadratures because, contrarily to many analytic solutions (including the one in Appendix A), all points away from the contour of the source region are numerically stable.

The $\Phi(\mathbf{x})$ function that describes the location of transformation strain is the same for anti-plane and in-plane strain problems, so the stress and strain components can be obtained using (5), (6), and (23). Figure 8 shows the combination of the 3 stress components obtained by deformation of a triangular source with 3 different components of transformation strain. I have checked that the results from the finite-difference and the numerical quadrature methods converge for these 9 cases.

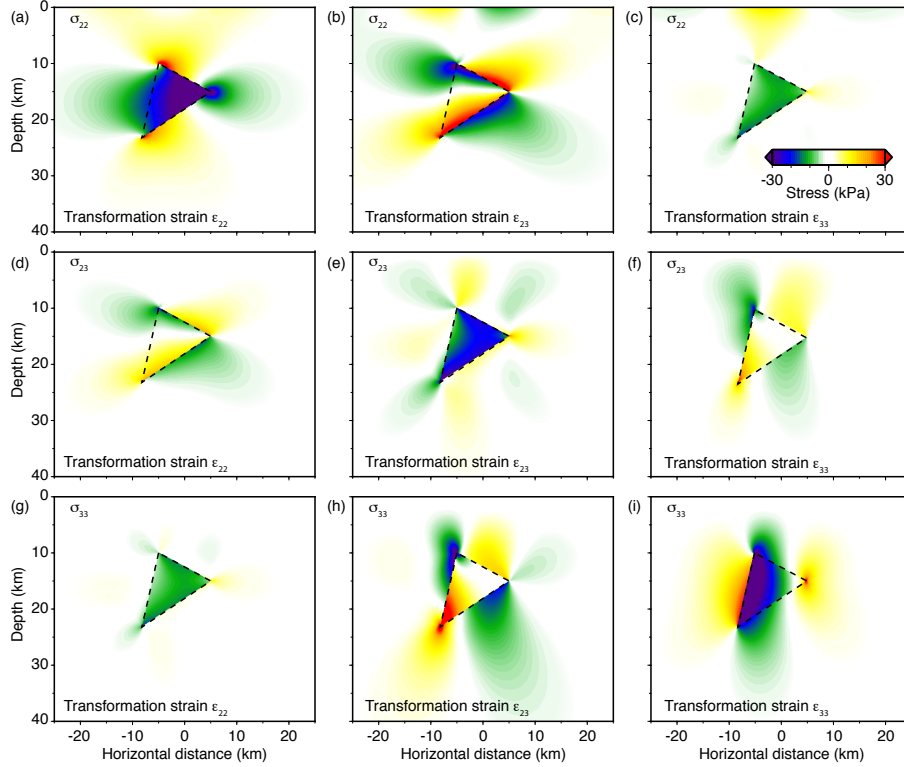


Figure 8: Stress field in plane strain due to anelastic strain confined in triangular elements (dashed triangles). The top panel with a), b), and c) show the horizontal stress. The middle panel with d), e), and f) show the shear stress. The bottom panel with g), h), and i) show the vertical stress. The left column with a), d), and g) are for the horizontal transformation strain $\epsilon_{22} = 10^{-6}$. The middle column with b), e), and h) are for a shear transformation strain of $\epsilon_{23} = 10^{-6}$. The right column with c), f), and i) is for a vertical transformation strain of $\epsilon_{33} = 10^{-6}$.

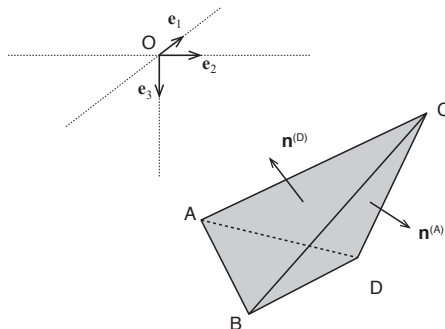


Figure 9: Three-dimensional deformation of a half-space due to anelastic strain confined in a tetrahedral element with vertices A, B, C, and D at coordinates \mathbf{x}^A , \mathbf{x}^B , \mathbf{x}^C , and \mathbf{x}^D , respectively. The normal vectors are pointing outwards, such that $\mathbf{n}^{(D)} \cdot (\mathbf{x}^D - \mathbf{x}^A) \leq 0$, $\mathbf{n}^{(D)} \cdot (\mathbf{x}^D - \mathbf{x}^B) \leq 0$, and $\mathbf{n}^{(D)} \cdot (\mathbf{x}^D - \mathbf{x}^C) \leq 0$.

Distributed deformation of tetrahedral strain volumes in three dimensions

The development of three-dimensional deformation models has afforded an increasingly accurate description of the mechanics of the lithosphere (*Aagaard et al.*, 2013; *Barbot et al.*, 2017; *Landry and Barbot*, 2016; *Mansinha and Smylie*, 1971; *McTigue and Segall*, 1988; *Meade*, 2007; *Nikkhoo and Walter*, 2015; *Okada*, 1985, 1992; *Sato and Matsu'ura*, 1974; *Wang et al.*, 2003). The expressions for the deformation induced by uniform transformation strain confined in a cuboid have been developed for a full elastic medium by *Faivre* (1969). *Chiu* (1978) derived the solution for certain components of displacement and strain at the surface of a half-space. *Barbot et al.* (2017) derived the displacement and stress everywhere in a half-space. The development of realistic rheological models of Earth's interior requires curvilinear meshes that conform to structural data, so in this manuscript I derive solutions for the case of transformation strain confined in a tetrahedral volume in a half-space, extending from the work of *Nozaki and Taya* (1997, 2001) for a full space.

Problem statement

I now consider deformation in a three-dimensional half-space (Figure 9). I consider a tetrahedral volume delineated by the vertices A, B, C, and D at coordinates \mathbf{x}^A , \mathbf{x}^B , \mathbf{x}^C , and \mathbf{x}^D , respectively, and subjected to the six independent transformation strain components

$$\boldsymbol{\epsilon}^i = \begin{pmatrix} \epsilon_{11} & \epsilon_{12} & \epsilon_{13} \\ \epsilon_{12} & \epsilon_{22} & \epsilon_{23} \\ \epsilon_{13} & \epsilon_{23} & \epsilon_{33} \end{pmatrix}. \quad (34)$$

Using (13), the deformation simplifies to

$$\begin{aligned}
u_i(x_1, x_2, x_3) &= \int_{\partial\Omega} G_{1i}(x_1, x_2, x_3; y_1, y_2, y_3) (m_{11}n_1 + m_{12}n_2 + m_{13}n_3) dy_1 dy_2 dy_3 \\
&+ \int_{\partial\Omega} G_{2i}(x_1, x_2, x_3; y_1, y_2, y_3) (m_{12}n_1 + m_{22}n_2 + m_{23}n_3) dy_1 dy_2 dy_3 \\
&+ \int_{\partial\Omega} G_{3i}(x_1, x_2, x_3; y_1, y_2, y_3) (m_{13}n_1 + m_{32}n_2 + m_{33}n_3) dy_1 dy_2 dy_3
\end{aligned} \tag{35}$$

for $i = 1, 2, 3$, where $G_{ij}(\mathbf{x}; \mathbf{y})$ represents the displacement component $u_j(\mathbf{x})$ induced by a point force in the \mathbf{e}_i direction located at \mathbf{y} . The Green's functions for the u_1 component are given by (Mindlin, 1936; Okada, 1985; Press, 1965; Segall, 2010)

$$\begin{aligned}
G_{11} &= \frac{1}{16\pi\mu(1-\nu)} \left[\frac{3-4\nu}{R_1} + \frac{1}{R_2} + \frac{(x_1-y_1)^2}{R_1^3} \right. \\
&\quad + \frac{(3-4\nu)(x_1-y_1)^2}{R_2^3} \\
&\quad + \frac{2x_3y_3(R_2^2-3(x_1-y_1)^2)}{R_2^5} \\
&\quad \left. + \frac{4(1-2\nu)(1-\nu)(R_2^2-(x_1-y_1)^2+R_2(x_3+y_3))}{R_2(R_2+x_3+y_3)^2} \right], \\
G_{21} &= \frac{(x_1-y_1)(x_2-y_2)}{16\pi\mu(1-\nu)} \left[\frac{1}{R_1^3} + \frac{3-4\nu}{R_2^3} - \frac{6x_3y_3}{R_2^5} - \frac{4(1-2\nu)(1-\nu)}{R_2(R_2+x_3+y_3)^2} \right], \\
G_{31} &= \frac{(x_1-y_1)}{16\pi\mu(1-\nu)} \left[\frac{x_3-y_3}{R_1^3} + \frac{(3-4\nu)(x_3-y_3)}{R_2^3} \right. \\
&\quad \left. + \frac{6x_3y_3(x_3+y_3)}{R_2^5} - \frac{4(1-2\nu)(1-\nu)}{R_2(R_2+x_3+y_3)} \right].
\end{aligned} \tag{36}$$

For the u_2 component, they are

$$\begin{aligned}
G_{12} &= \frac{(x_1 - y_1)(x_2 - y_2)}{16\pi\mu(1 - \nu)} \left[\frac{1}{R_1^3} + \frac{3 - 4\nu}{R_2^3} - \frac{6x_3y_3}{R_2^5} - \frac{4(1 - 2\nu)(1 - \nu)}{R_2(R_2 + x_3 + y_3)^2} \right], \\
G_{22} &= \frac{1}{16\pi\mu(1 - \nu)} \left[\frac{3 - 4\nu}{R_1} + \frac{1}{R_2} \right. \\
&\quad + \frac{(x_2 - y_2)^2}{R_1^3} + \frac{(3 - 4\nu)(x_2 - y_2)^2}{R_2^3} \\
&\quad + \frac{2x_3y_3(R_2^2 - 3(x_2 - y_2)^2)}{R_2^5} \\
&\quad \left. + \frac{4(1 - 2\nu)(1 - \nu)(R_2^2 - (x_2 - y_2)^2 + R_2(x_3 + y_3))}{R_2(R_2 + x_3 + y_3)^2} \right], \\
G_{32} &= \frac{(x_2 - y_2)}{16\pi\mu(1 - \nu)} \left[\frac{x_3 - y_3}{R_1^3} + \frac{(3 - 4\nu)(x_3 - y_3)}{R_2^3} \right. \\
&\quad \left. + \frac{6x_3y_3(x_3 + y_3)}{R_2^5} - \frac{4(1 - 2\nu)(1 - \nu)}{R_2(R_2 + x_3 + y_3)} \right]. \tag{37}
\end{aligned}$$

For the displacement component u_3 , they are given by

$$\begin{aligned}
G_{13} &= \frac{(x_1 - y_1)}{16\pi\mu(1 - \nu)} \left[\frac{x_3 - y_3}{R_1^3} + \frac{(3 - 4\nu)(x_3 - y_3)}{R_2^3} \right. \\
&\quad \left. - \frac{6x_3y_3(x_3 + y_3)}{R_2^5} + \frac{4(1 - 2\nu)(1 - \nu)}{R_2(R_2 + x_3 + y_3)} \right], \\
G_{23} &= \frac{(x_2 - y_2)}{16\pi\mu(1 - \nu)} \left[\frac{x_3 - y_3}{R_1^3} + \frac{(3 - 4\nu)(x_3 - y_3)}{R_2^3} \right. \\
&\quad \left. - \frac{6x_3y_3(x_3 + y_3)}{R_2^5} + \frac{4(1 - 2\nu)(1 - \nu)}{R_2(R_2 + x_3 + y_3)} \right] \\
G_{33} &= \frac{1}{16\pi\mu(1 - \nu)} \left[\frac{3 - 4\nu}{R_1} + \frac{5 - 12\nu + 8\nu^2}{R_2} + \frac{(x_3 - y_3)^2}{R_1^3} \right. \\
&\quad \left. + \frac{6x_3y_3(x_3 + y_3)^2}{R_2^5} + \frac{(3 - 4\nu)(x_3 + y_3)^2 - 2x_3y_3}{R_2^3} \right]. \tag{38}
\end{aligned}$$

All involve the radii

$$\begin{aligned}
R_1 &= ((x_1 - y_1)^2 + (x_2 - y_2)^2 + (y_3 - x_3)^2)^{1/2} \\
R_2 &= ((x_1 - y_1)^2 + (x_2 - y_2)^2 + (x_3 + y_3)^2)^{1/2}. \tag{39}
\end{aligned}$$

Semi-analytic solution with the double-exponential and the Gauss-Legendre quadratures

The integral (35) involves surface integrals of the form (no summation implied over the indices i and j)

$$K_{ij} = \int_{\partial\Omega} G_{ij}(x_1, x_2, x_3; y_1, y_2, y_3) (m_{i1}n_1 + m_{i2}n_2 + m_{i3}n_3) dy_1 dy_2 dy_3 , \quad (40)$$

that can be broken down into the four faces ABC , BCD , CDA , and DAB of the tetrahedron, as follows

$$\begin{aligned} K_{ij} = & \left(m_{i1}n_1^{(D)} + m_{i2}n_2^{(D)} + m_{i3}n_3^{(D)} \right) \int_{ABC} G_{ij}(x_1, x_2, x_3; y_1, y_2, y_3) dy_1 dy_2 dy_3 \\ & + \left(m_{i1}n_1^{(A)} + m_{i2}n_2^{(A)} + m_{i3}n_3^{(A)} \right) \int_{BCD} G_{ij}(x_1, x_2, x_3; y_1, y_2, y_3) dy_1 dy_2 dy_3 \\ & + \left(m_{i1}n_1^{(B)} + m_{i2}n_2^{(B)} + m_{i3}n_3^{(B)} \right) \int_{CDA} G_{ij}(x_1, x_2, x_3; y_1, y_2, y_3) dy_1 dy_2 dy_3 \\ & + \left(m_{i1}n_1^{(C)} + m_{i2}n_2^{(C)} + m_{i3}n_3^{(C)} \right) \int_{DAB} G_{ij}(x_1, x_2, x_3; y_1, y_2, y_3) dy_1 dy_2 dy_3 . \end{aligned} \quad (41)$$

Following the approach described in the previous sections, I obtain solutions to the surface integrals (41) using the double-exponential and the Gauss-Legendre quadratures. To do so, I consider the individual surface integral

$$J_{ij}(x_1, x_2, x_3) = \int_{ABC} G_{ij}(x_1, x_2, x_3; y_1, y_2, y_3) dy_1 dy_2 dy_3 , \quad (42)$$

which I write as a parameterized surface integral and in canonical form, to get

$$J_{ij}(x_1, x_2, x_3) = \frac{\mathcal{A}}{4} \int_{-1}^1 \int_{-1}^1 (1-v) G_{ij}(x_1, x_2, x_3; y_1(u, v), y_2(u, v), y_3(u, v)) du dv , \quad (43)$$

where \mathcal{A} is the area of the triangle ABC and u and v are dummy variables of integration. The parameterization

$$\begin{aligned} \mathbf{y}(u, v) = & \frac{1}{4} \mathbf{x}^A (1-u)(1-v) \\ & + \frac{1}{4} \mathbf{x}^B (1+u)(1-v) \\ & + \frac{1}{2} \mathbf{x}^C (1+v) . \end{aligned} \quad (44)$$

maps the triangle ABC in three-dimensional space to a right isosceles triangle in the uv space (e.g., *Beer et al.*, 2008; *Pozrikidis*, 2002), where \mathbf{x}^A , \mathbf{x}^B , and \mathbf{x}^C are the spatial coordinates of vertices A , B , and C in integral (42), respectively.

For each displacement component correspond twelve integrals such as (43) due to the presence of three force components on four faces. Therefore, the displacement field requires the evaluation of at most 36 surface integrals. Examples

of surface displacements in map view caused by anelastic strain confined in a tetrahedron are shown in Figure 10. The vertices are located at $A = (-5, -5, 5)$, $B = (-5, 5, 5)$, $C = (-5, 5, 15)$, and $D = (5, 5, 5)$ expressed in km. Each panel shows the displacement caused by a single transformation strain component with an amplitude of one microstrain.

Six tetrahedra can be arranged to form a cuboid. In this case the semi-analytic solution agrees with the analytical solution of *Barbot et al.* (2017) to the limit of double-precision floating point accuracy. As the numerical solution involves a surface integral, the computational burden is much larger than for the two-dimensional case with only line integrals. The double-exponential quadrature with 601 integration points takes about 2,500 times longer than the analytic solution for a cuboid source. In contrast, the Gauss-Legendre quadrature with 7 and 15 points in both directions takes only 3 times and 16 times longer than the analytic solution, respectively. As the solution based on the Gauss-Legendre quadrature offers the same accuracy but is free of numerical artifacts away from the surface of the tetrahedron, the small difference in computational cost makes this approach more appealing than using the analytic solution.

Stress and strain

The stress field is essential to simulate forward models of deformation with the integral method (*Barbot*, 2018) and to regularize inverse problems involving distributed strain (*Qiu et al.*, 2018). The strain can be obtained by differencing the displacement field obtained with (35) but a more accurate approach is to directly integrate the Green's functions for the displacement gradient, as in

$$u_{i,j}(x_1, x_2, x_3) = \int_{\partial\Omega} G_{ki,j}(x_1, x_2, x_3; y_1, y_2, y_3) m_{kl} n_l dy_1 dy_2 dy_3 . \quad (45)$$

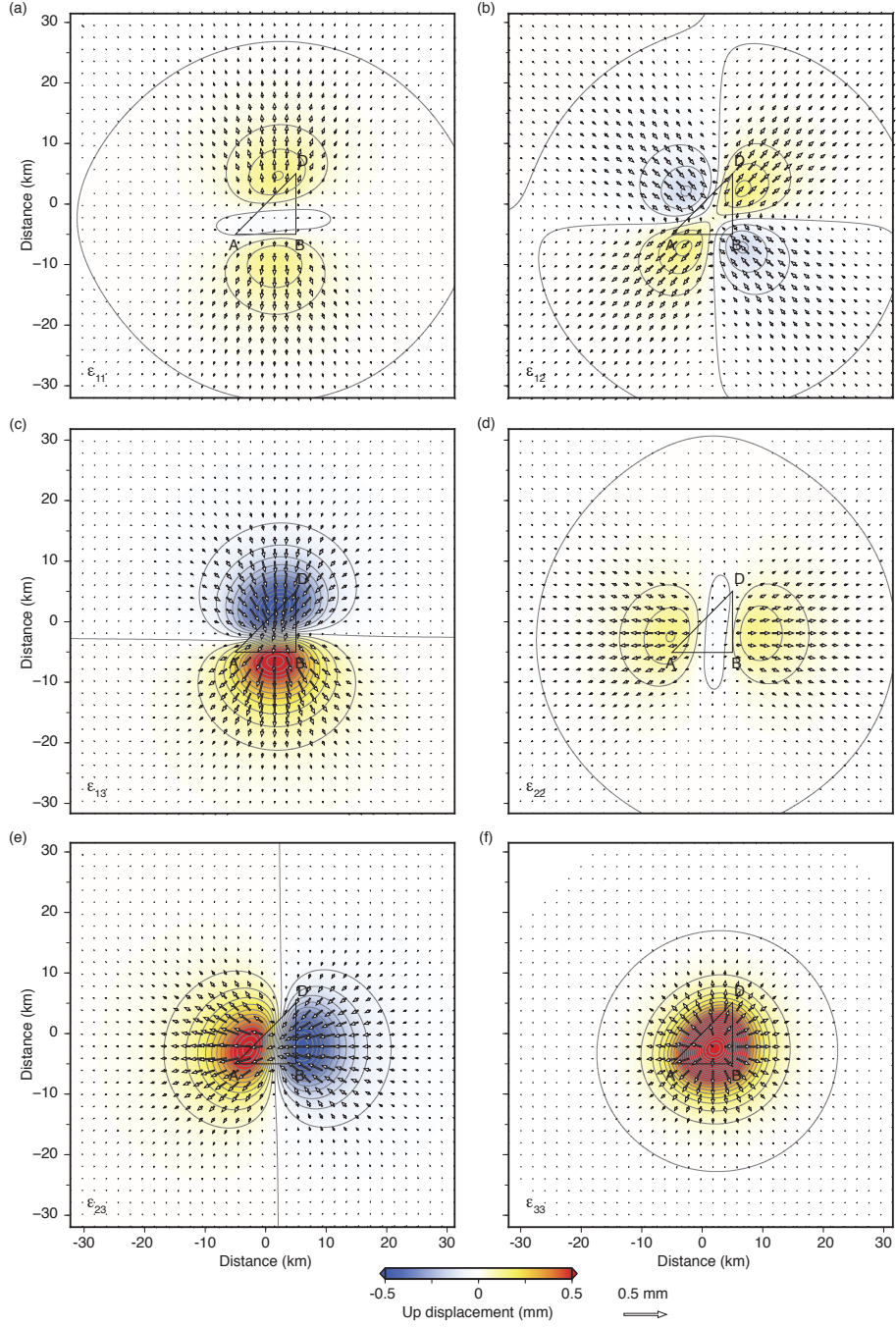


Figure 10: Displacement field at the surface of the half-space due to anelastic strain confined in a tetrahedral volume ABCD. The arrows indicate horizontal displacements and the background indicates the vertical (positive up) displacement. The panels corresponds to different components of transformation strain with an amplitude of one microstrain: a) uniaxial strain ϵ_{11} , b) pure shear ϵ_{12} , c) vertical pure shear ϵ_{13} , d) horizontal uniaxial extension ϵ_{22} , e) vertical pure shear ϵ_{23} , and f) vertical extension ϵ_{33} . The contours (dashed lines) are every 0.05 mm.

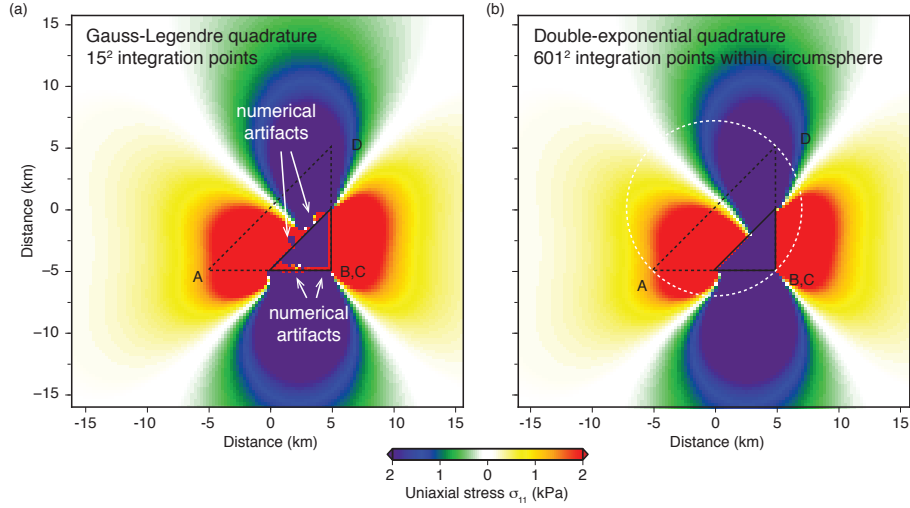


Figure 11: Uniaxial stress component σ_{11} due to non-trivial anelastic strain component ϵ_{11} evaluated with a) the Gauss-Legendre quadrature throughout the domain with 15^2 integration points (15 points in each direction of integration of the 4 triangular surfaces) and b) the double-exponential quadrature within the circumsphere (horizontal footprint in dashed white circle) using 601^2 integration points and the Gauss-Legendre quadrature outside the circumsphere. In both cases, the tetrahedron connects the vertices $A = (-5, -5, 5)$, $B = (-5, 5, 5)$, $C = (-5, 5, 15)$, and $D = (5, 5, 5)$ expressed in km (horizontal footprint in dashed black profile) and the figure shows horizontal cross-sections cutting through the tetrahedron at 10 km depth. The intersection of the cross-section and the tetrahedron is a triangle surface (contour in black profile.) Numerical artifacts near the surface of the tetrahedron are evident with the solution based on the Gauss-Legendre quadrature. They are mostly eliminated with the double-exponential quadrature.

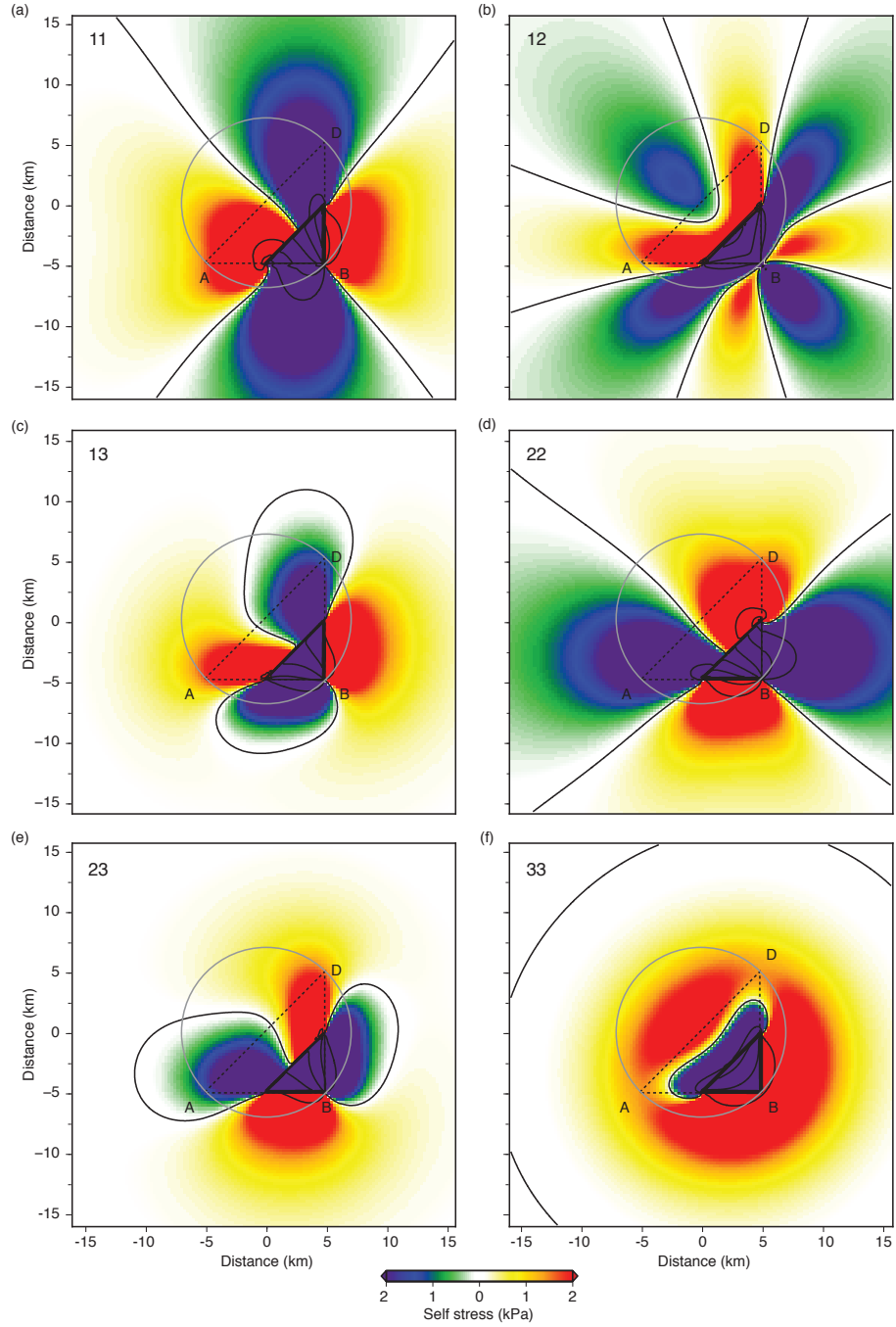


Figure 12: The stress component σ_{ij} in horizontal cross-section due to the nontrivial transformation strain component ϵ_{ij} confined in a tetrahedron (self-stress). The surface footprint of the tetrahedron is shown in the dashed profile. The intersection of the cross-section with the tetrahedron is shown in solid black profile. The double-exponential quadrature is used for points within the circumsphere (horizontal footprint shown in grey circle) and the Gauss-Legendre quadrature is used outside. The panels correspond to different components of transformation strain with an amplitude of one microstrain: a) uniaxial stress σ_{11} due to nontrivial transformation strain component ϵ_{11} , b) stress component σ_{12} due to pure shear ϵ_{12} in the tetrahedron, c) stress component σ_{13} due to vertical pure shear ϵ_{13} , d) σ_{22} due to horizontal uniaxial extension ϵ_{22} , e) stress component σ_{23} due to vertical pure shear ϵ_{23} , and f) vertical stress σ_{33} due to vertical extension ϵ_{33} within the tetrahedron. The contours (dashed lines) are every 10 kPa.

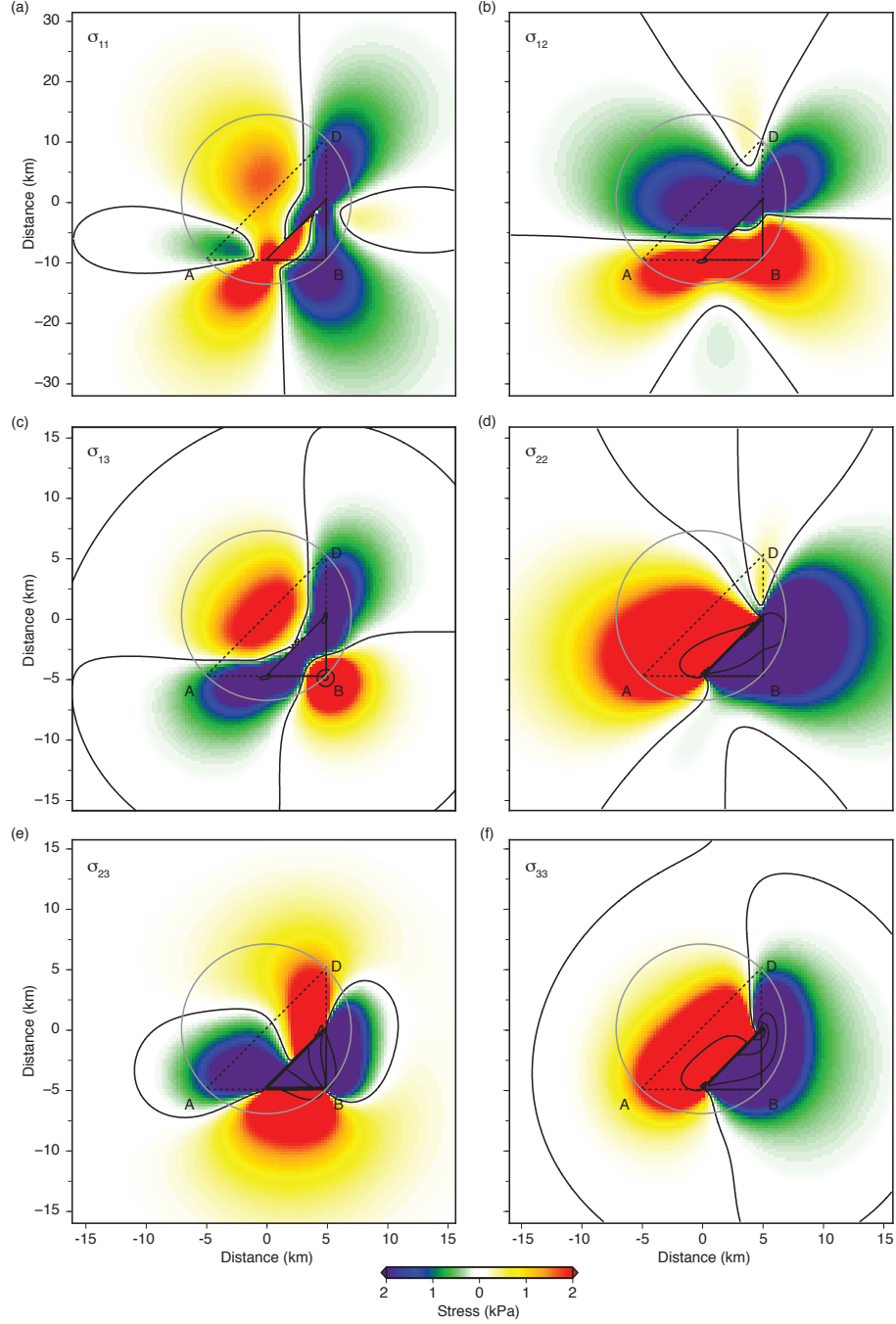


Figure 13: The stress field in horizontal cross-section due to the nontrivial transformation strain component ϵ_{23} (one microstrain) confined in a tetrahedron. The surface footprint of the tetrahedron is shown in the dashed profile. The intersection of the cross-section with the tetrahedron is shown in solid black profile. The double-exponential and the Gauss-Legendre quadratures are used for points inside, respectively outside, the circumsphere (horizontal footprint shown in grey circle). a) uniaxial stress σ_{11} , b) shear stress component σ_{12} , c) shear stress component σ_{13} , d) horizontal uniaxial stress component σ_{22} , e) vertical shear stress component σ_{23} , and F) vertical stress σ_{33} . The contours (dashed lines) are every 10 kPa.

The derivatives of the Green's function are given in closed form below for completeness,

$$\begin{aligned}
G_{11,1} &= \frac{(x_1 - y_1)}{16\pi\mu(1-\nu)} \left[-\frac{(3-4\nu)}{R_1^3} - \frac{1}{R_2^3} + \frac{2R_1^2 - 3(x_1 - y_1)^2}{R_1^5} \right. \\
&\quad + (3-4\nu) \frac{2R_2^2 - 3(x_1 - y_1)^2}{R_2^5} - 6y_3x_3 \frac{3R_2^2 - 5(x_1 - y_1)^2}{R_2^7} \\
&\quad - 12 \frac{(1-2\nu)(1-\nu)}{R_2(R_2 + x_3 + y_3)^2} \\
&\quad \left. + \frac{4(1-2\nu)(1-\nu)(x_1 - y_1)^2}{R_2^3(R_2 + x_3 + y_3)^2} + \frac{8(1-2\nu)(1-\nu)(x_1 - y_1)^2}{R_2^2(R_2 + x_3 + y_3)^3} \right], \\
G_{11,2} &= \frac{(x_2 - y_2)}{16\pi\mu(1-\nu)} \left[-\frac{(3-4\nu)}{R_1^3} - \frac{1}{R_2^3} - \frac{3(x_1 - y_1)^2}{R_1^5} - \frac{3(3-4\nu)(x_1 - y_1)^2}{R_2^5} \right. \\
&\quad - 6y_3x_3 \frac{R_2^2 - 5(x_1 - y_1)^2}{R_2^7} - \frac{4(1-2\nu)(1-\nu)}{R_2(R_2 + x_3 + y_3)^2} \\
&\quad \left. + 4(1-2\nu)(1-\nu)(x_1 - y_1)^2 \frac{3R_2 + x_3 + y_3}{R_2^3(R_2 + x_3 + y_3)^3} \right], \\
G_{11,3} &= \frac{1}{16\pi\mu(1-\nu)} \left[-\frac{(3-4\nu)(x_3 - y_3)}{R_1^3} - \frac{(x_3 + y_3)}{R_2^3} - 3 \frac{(x_1 - y_1)^2(x_3 - y_3)}{R_1^5} \right. \\
&\quad - 3 \frac{(3-4\nu)(x_1 - y_1)^2(x_3 + y_3)}{R_2^5} \\
&\quad + 2y_3 \frac{R_2^2 - 3x_3(x_3 + y_3)}{R_2^5} \\
&\quad - 6y_3(x_1 - y_1)^2 \frac{R_2^2 - 5x_3(x_3 + y_3)}{R_2^7} \\
&\quad - 4 \frac{(1-2\nu)(1-\nu)}{R_2(R_2 + x_3 + y_3)} \\
&\quad \left. + 4(1-2\nu)(1-\nu)(x_1 - y_1)^2 \frac{2R_2 + x_3 + y_3}{R_2^3(R_2 + x_3 + y_3)^2} \right], \tag{46}
\end{aligned}$$

and

$$\begin{aligned}
G_{21,1} &= \frac{(x_2 - y_2)}{16\pi\mu(1 - \nu)} \left[\frac{R_1^2 - 3(x_1 - y_1)^2}{R_1^5} + (3 - 4\nu) \frac{R_2^2 - 3(x_1 - y_1)^2}{R_2^5} \right. \\
&\quad - 6y_3x_3 \frac{R_2^2 - 5(x_1 - y_1)^2}{R_2^7} - \frac{4(1 - 2\nu)(1 - \nu)}{R_2(R_2 + x_3 + y_3)^2} \\
&\quad \left. + 4(1 - 2\nu)(1 - \nu)(x_1 - y_1)^2 \frac{3R_2 + x_3 + y_3}{R_2^3(R_2 + x_3 + y_3)^3} \right], \\
G_{21,2} &= \frac{(x_1 - y_1)}{16\pi\mu(1 - \nu)} \left[\frac{R_1^2 - 3(x_2 - y_2)^2}{R_1^5} + (3 - 4\nu) \frac{R_2^2 - 3(x_2 - y_2)^2}{R_2^5} \right. \\
&\quad - 6y_3x_3 \frac{R_2^2 - 5(x_2 - y_2)^2}{R_2^7} - \frac{4(1 - 2\nu)(1 - \nu)}{R_2(R_2 + x_3 + y_3)^2} \\
&\quad \left. + 4(1 - 2\nu)(1 - \nu)(x_2 - y_2)^2 \frac{3R_2 + x_3 + y_3}{R_2^3(R_2 + x_3 + y_3)^3} \right], \\
G_{21,3} &= \frac{(x_1 - y_1)(x_2 - y_2)}{16\pi\mu(1 - \nu)} \left[-3 \frac{(x_3 - y_3)}{R_1^5} - 3(3 - 4\nu) \frac{(x_3 + y_3)}{R_2^5} \right. \\
&\quad - 6y_3 \frac{R_2^2 - 5x_3(x_3 + y_3)}{R_2^7} \\
&\quad \left. + 4(1 - 2\nu)(1 - \nu) \frac{2R_2 + x_3 + y_3}{R_2^3(R_2 + x_3 + y_3)^2} \right]. \tag{47}
\end{aligned}$$

Continuing,

$$\begin{aligned}
G_{31,1} &= \frac{1}{16\pi\mu(1-\nu)} \left[(x_3 - y_3) \frac{R_1^2 - 3(x_1 - y_1)^2}{R_1^5} \right. \\
&\quad + (3 - 4\nu)(x_3 - y_3) \frac{R_2^2 - 3(x_1 - y_1)^2}{R_2^5} \\
&\quad + 6x_3y_3(x_3 + y_3) \frac{R_2^2 - 5(x_1 - y_1)^2}{R_2^7} \\
&\quad - 4(1 - 2\nu)(1 - \nu) \frac{1}{R_2(R_2 + x_3 + y_3)} \\
&\quad \left. + 4(1 - 2\nu)(1 - \nu)(x_1 - y_1)^2 \frac{2R_2 + x_3 + y_3}{R_2^3(R_2 + x_3 + y_3)^2} \right], \\
G_{31,2} &= \frac{(x_1 - y_1)(x_2 - y_2)}{16\pi\mu(1-\nu)} \left[-3 \frac{(x_3 - y_3)}{R_1^5} - 3(3 - 4\nu) \frac{(x_3 - y_3)}{R_2^5} \right. \\
&\quad \left. - 30y_3x_3 \frac{(x_3 + y_3)}{R_2^7} + 4(1 - 2\nu)(1 - \nu) \frac{2R_2 + x_3 + y_3}{R_2^3(R_2 + x_3 + y_3)^2} \right], \\
G_{31,3} &= \frac{(x_1 - y_1)}{16\pi\mu(1-\nu)} \left[\frac{R_1^2 - 3(x_3 - y_3)^2}{R_1^5} + (3 - 4\nu) \frac{R_2^2 - 3(x_3 + y_3)(x_3 - y_3)}{R_2^5} \right. \\
&\quad \left. + 6y_3 \frac{R_2^2(2x_3 + y_3) - 5x_3(x_3 + y_3)^2}{R_2^7} + 4 \frac{(1 - 2\nu)(1 - \nu)}{R_2^3} \right].
\end{aligned} \tag{48}$$

The derivatives of the G_{12} component are the same as for G_{21} component

$$\begin{aligned}
G_{12,1} &= \frac{(x_2 - y_2)}{16\pi\mu(1-\nu)} \left[\frac{R_1^2 - 3(x_1 - y_1)^2}{R_1^5} + (3 - 4\nu) \frac{R_2^2 - 3(x_1 - y_1)^2}{R_2^5} \right. \\
&\quad - 6 y_3 x_3 \frac{R_2^2 - 5(x_1 - y_1)^2}{R_2^7} - \frac{4(1-\nu)(1-2\nu)}{R_2(R_2 + x_3 + y_3)^2} \\
&\quad \left. + 4(1-\nu)(1-2\nu)(x_1 - y_1)^2 \frac{3R_2 + x_3 + y_3}{R_2^3(R_2 + x_3 + y_3)^3} \right], \\
G_{12,2} &= \frac{(x_1 - y_1)}{16\pi\mu(1-\nu)} \left[\frac{R_1^2 - 3(x_2 - y_2)^2}{R_1^5} + (3 - 4\nu) \frac{R_2^2 - 3(x_2 - y_2)^2}{R_2^5} \right. \\
&\quad - 6 y_3 x_3 \frac{R_2^2 - 5(x_2 - y_2)^2}{R_2^7} - \frac{4(1-\nu)(1-2\nu)}{R_2(R_2 + x_3 + y_3)^2} \\
&\quad \left. + 4(1-\nu)(1-2\nu)(x_2 - y_2)^2 \frac{3R_2 + x_3 + y_3}{R_2^3(R_2 + x_3 + y_3)^3} \right], \\
G_{12,3} &= \frac{(x_1 - y_1)(x_2 - y_2)}{16\pi\mu(1-\nu)} \left[-3 \frac{(x_3 - y_3)}{R_1^5} - 3(3 - 4\nu) \frac{(x_3 + y_3)}{R_2^5} \right. \\
&\quad - 6 y_3 \frac{R_2^2 - 5x_3(x_3 + y_3)}{R_2^7} \\
&\quad \left. + 4(1 - 2\nu)(1 - \nu) \frac{2R_2 + x_3 + y_3}{R_2^3(R_2 + x_3 + y_3)^2} \right]. \tag{49}
\end{aligned}$$

The derivatives of the G_{22} have a symmetry with those of the G_{11} component by permutation of the 1 and 2 indices

$$\begin{aligned}
G_{22,1} &= \frac{(x_1 - y_1)}{16\pi\mu(1-\nu)} \left[-\frac{(3-4\nu)}{R_1^3} - \frac{1}{R_2^3} - \frac{3(x_2 - y_2)^2}{R_1^5} - \frac{3(3-4\nu)(x_2 - y_2)^2}{R_2^5} \right. \\
&\quad \left. - 6y_3x_3 \frac{R_2^2 - 5(x_2 - y_2)^2}{R_2^7} - \frac{4(1-2\nu)(1-\nu)}{R_2(R_2 + x_3 + y_3)^2} \right. \\
&\quad \left. + 4(1-2\nu)(1-\nu)(x_2 - y_2)^2 \frac{3R_2 + x_3 + y_3}{R_2^3(R_2 + x_3 + y_3)^3} \right], \\
G_{22,2} &= \frac{(x_2 - y_2)}{16\pi\mu(1-\nu)} \left[-\frac{(3-4\nu)}{R_1^3} - \frac{1}{R_2^3} + \frac{2R_1^2 - 3(x_2 - y_2)^2}{R_1^5} \right. \\
&\quad \left. + (3-4\nu) \frac{2R_2^2 - 3(x_2 - y_2)^2}{R_2^5} - 6y_3x_3 \frac{3R_2^2 - 5(x_2 - y_2)^2}{R_2^7} \right. \\
&\quad \left. - 12 \frac{(1-2\nu)(1-\nu)}{R_2(R_2 + x_3 + y_3)^2} \right. \\
&\quad \left. + 4(1-2\nu)(1-\nu)(x_2 - y_2)^2 \frac{3R_2 + x_3 + y_3}{R_2^3(R_2 + x_3 + y_3)^3} \right], \\
G_{22,3} &= \frac{1}{16\pi\mu(1-\nu)} \left[-(3-4\nu) \frac{(x_3 - y_3)}{R_1^3} - \frac{(x_3 + y_3)}{R_2^3} - 3 \frac{(x_2 - y_2)^2(x_3 - y_3)}{R_1^5} \right. \\
&\quad \left. - 3(3-4\nu) \frac{(x_2 - y_2)^2(x_3 + y_3)}{R_2^5} \right. \\
&\quad \left. + 2y_3 \frac{R_2^2 - 3x_3(x_3 + y_3)}{R_2^5} \right. \\
&\quad \left. - 6y_3(x_2 - y_2)^2 \frac{R_2^2 - 5x_3(x_3 + y_3)}{R_2^7} \right. \\
&\quad \left. - 4 \frac{(1-2\nu)(1-\nu)}{R_2(R_2 + x_3 + y_3)} \right. \\
&\quad \left. + 4(1-2\nu)(1-\nu)(x_2 - y_2)^2 \frac{2R_2 + x_3 + y_3}{R_2^3(R_2 + x_3 + y_3)^2} \right], \tag{50}
\end{aligned}$$

The derivatives of the G_{32} term can be obtained from the G_{31} term by permutation of the 1 and 2 indices,

$$\begin{aligned}
G_{32,1} &= \frac{(x_1 - y_1)(x_2 - y_2)}{16\pi\mu(1 - \nu)} \left[-3 \frac{(x_3 - y_3)}{R_1^5} - 3(3 - 4\nu) \frac{(x_3 - y_3)}{R_2^5} \right. \\
&\quad \left. - 30 y_3 x_3 \frac{(x_3 + y_3)}{R_2^7} + 4(1 - 2\nu)(1 - \nu) \frac{2R_2 + x_3 + y_3}{R_2^3(R_2 + x_3 + y_3)^2} \right], \\
G_{32,2} &= \frac{1}{16\pi\mu(1 - \nu)} \left[(x_3 - y_3) \frac{R_1^2 - 3(x_2 - y_2)^2}{R_1^5} \right. \\
&\quad + (3 - 4\nu)(x_3 - y_3) \frac{R_2^2 - 3(x_2 - y_2)^2}{R_2^5} \\
&\quad + 6 y_3 x_3 (x_3 + y_3) \frac{R_2^2 - 5(x_2 - y_2)^2}{R_2^7} \\
&\quad - 4(1 - 2\nu)(1 - \nu) \frac{1}{R_2(R_2 + x_3 + y_3)} \\
&\quad \left. + 4(1 - 2\nu)(1 - \nu)(x_2 - y_2)^2 \frac{2R_2 + x_3 + y_3}{R_2^3(R_2 + x_3 + y_3)^2} \right], \\
G_{32,3} &= \frac{(x_2 - y_2)}{16\pi\mu(1 - \nu)} \left[\frac{R_1^2 - 3(x_3 - y_3)^2}{R_1^5} + (3 - 4\nu) \frac{R_2^2 - 3(x_3 - y_3)(x_3 + y_3)}{R_2^5} \right. \\
&\quad \left. + 6 y_3 \frac{(2x_3 + y_3)}{R_2^5} - 30 y_3 x_3 \frac{(x_3 + y_3)^2}{R_2^7} + 4 \frac{(1 - 2\nu)(1 - \nu)}{R_2^3} \right].
\end{aligned} \tag{51}$$

The derivatives of the G_{13} component are

$$\begin{aligned}
G_{13,1} &= \frac{1}{16\pi\mu(1-\nu)} \left[(x_3 - y_3) \frac{R_1^2 - 3(x_1 - y_1)^2}{R_1^5} \right. \\
&\quad + (3 - 4\nu)(x_3 - y_3) \frac{R_2^2 - 3(x_1 - y_1)^2}{R_2^5} \\
&\quad - 6y_3x_3(x_3 + y_3) \frac{R_2^2 - 5(x_1 - y_1)^2}{R_2^7} + \frac{4(1 - 2\nu)(1 - \nu)}{R_2(R_2 + x_3 + y_3)} \\
&\quad \left. - 4(1 - 2\nu)(1 - \nu)(x_1 - y_1)^2 \frac{2R_2 + x_3 + y_3}{R_2^3(R_2 + x_3 + y_3)^2} \right], \\
G_{13,2} &= \frac{(x_1 - y_1)(x_2 - y_2)}{16\pi\mu(1 - \nu)} \left[-3(x_3 - y_3) \frac{1}{R_1^5} \right. \\
&\quad - 3(3 - 4\nu)(x_3 - y_3) \frac{1}{R_2^5} \\
&\quad + 30y_3x_3(x_3 + y_3) \frac{1}{R_2^7} \\
&\quad \left. - 4(1 - 2\nu)(1 - \nu) \frac{2R_2 + x_3 + y_3}{R_2^3(R_2 + x_3 + y_3)^2} \right], \\
G_{13,3} &= \frac{(x_1 - y_1)}{16\pi\mu(1 - \nu)} \left[\frac{R_1^2 - 3(x_3 - y_3)^2}{R_1^5} \right. \\
&\quad + (3 - 4\nu) \frac{R_2^2 - 3(x_3 - y_3)(x_3 + y_3)}{R_2^5} \\
&\quad - 6y_3 \frac{2x_3 + y_3}{R_2^5} + 30y_3x_3 \frac{(x_3 + y_3)^2}{R_2^7} \\
&\quad \left. - 4(1 - 2\nu)(1 - \nu) \frac{1}{R_2^3} \right].
\end{aligned} \tag{52}$$

The derivatives of the G_{23} can be obtained from the G_{13} derivatives by permutation of the 1 and 2 indices

$$\begin{aligned}
G_{23,1} &= \frac{(x_1 - y_1)(x_2 - y_2)}{16\pi\mu(1 - \nu)} \left[-3(x_3 - y_3) \frac{1}{R_1^5} \right. \\
&\quad - 3(3 - 4\nu)(x_3 - y_3) \frac{1}{R_2^5} \\
&\quad + 30y_3x_3(x_3 + y_3) \frac{1}{R_2^7} \\
&\quad \left. - 4(1 - 2\nu)(1 - \nu) \frac{2R_2 + x_3 + y_3}{R_2^3(R_2 + x_3 + y_3)^2} \right], \\
G_{23,2} &= \frac{1}{16\pi\mu(1 - \nu)} \left[(x_3 - y_3) \frac{R_1^2 - 3(x_2 - y_2)^2}{R_1^5} \right. \\
&\quad + (3 - 4\nu)(x_3 - y_3) \frac{R_2^2 - 3(x_2 - y_2)^2}{R_2^5} \\
&\quad - 6y_3x_3(x_3 + y_3) \frac{R_2^2 - 5(x_2 - y_2)^2}{R_2^7} + \frac{4(1 - 2\nu)(1 - \nu)}{R_2(R_2 + x_3 + y_3)} \\
&\quad \left. - 4(1 - 2\nu)(1 - \nu)(x_2 - y_2)^2 \frac{2R_2 + x_3 + y_3}{R_2^3(R_2 + x_3 + y_3)^2} \right], \\
G_{23,3} &= \frac{(x_2 - y_2)}{16\pi\mu(1 - \nu)} \left[\frac{R_1^2 - 3(x_3 - y_3)^2}{R_1^5} \right. \\
&\quad + (3 - 4\nu) \frac{R_2^2 - 3(x_3 - y_3)(x_3 + y_3)}{R_2^5} \\
&\quad - 6y_3 \frac{2x_3 + y_3}{R_2^5} + 6y_3x_3 \frac{(x_3 + y_3)^2}{R_2^7} \\
&\quad \left. - 4(1 - 2\nu)(1 - \nu) \frac{1}{R_2^3} \right].
\end{aligned} \tag{53}$$

Finally, the derivatives of the G_{33} component are

$$\begin{aligned}
G_{33,1} &= \frac{(x_1 - y_1)}{16\pi\mu(1 - \nu)} \left[- (3 - 4\nu) \frac{1}{R_1^3} \right. \\
&\quad - (5 - 12\nu + 8\nu^2) \frac{1}{R_2^3} \\
&\quad - 3 \frac{(x_3 - y_3)^2}{R_1^5} - 30 y_3 x_3 \frac{(x_3 + y_3)^2}{R_2^7} \\
&\quad \left. - 3(3 - 4\nu) \frac{(x_3 + y_3)^2}{R_2^5} + 6 \frac{y_3 x_3}{R_2^5} \right], \\
G_{33,2} &= \frac{(x_2 - y_2)}{16\pi\mu(1 - \nu)} \left[- (3 - 4\nu) \frac{1}{R_1^3} \right. \\
&\quad - (5 - 12\nu + 8\nu^2) \frac{1}{R_2^3} \\
&\quad - 3 \frac{(x_3 - y_3)^2}{R_1^5} - 30 y_3 x_3 \frac{(x_3 + y_3)^2}{R_2^7} \\
&\quad \left. - 3(3 - 4\nu) \frac{(x_3 + y_3)^2}{R_2^5} + 6 \frac{y_3 x_3}{R_2^5} \right], \\
G_{33,3} &= \frac{1}{16\pi\mu(1 - \nu)} \left[- (3 - 4\nu) \frac{(x_3 - y_3)}{R_1^3} \right. \\
&\quad - (5 - 12\nu + 8\nu^2) \frac{(x_3 + y_3)}{R_2^3} \\
&\quad + (x_3 - y_3) \frac{2R_1^2 - 3(x_3 - y_3)^2}{R_1^5} + 6 y_3 \frac{(x_3 + y_3)^2}{R_2^5} \\
&\quad + 6 y_3 x_3 (x_3 + y_3) \frac{2R_2^2 - 5(x_3 + y_3)^2}{R_2^7} \\
&\quad + (3 - 4\nu) (x_3 + y_3) \frac{2R_2^2 - 3(x_3 + y_3)^2}{R_2^5} \\
&\quad \left. - 2 y_3 \frac{R_2^2 - 3x_3(x_3 + y_3)}{R_2^5} \right].
\end{aligned} \tag{54}$$

In all the terms composing the Green's functions (36-38) and their derivatives (46-54), the only singular point is at $\mathbf{x} = \mathbf{y}$, guaranteeing that the numerical integration of the Green's functions or their derivatives will be numerically stable at any point away from the surface compounding the source.

For a tetrahedral region with vertices A, B, C, and D as in Figure 9, the location of the transformation strain is given by the product of four Heaviside

functions

$$\begin{aligned}
\Phi(\mathbf{x}) = & H \left[\left(\frac{\mathbf{x}^A + \mathbf{x}^B + \mathbf{x}^C}{3} - \mathbf{x} \right) \cdot \mathbf{n}^{(D)} \right] \\
& \times H \left[\left(\frac{\mathbf{x}^B + \mathbf{x}^C + \mathbf{x}^D}{3} - \mathbf{x} \right) \cdot \mathbf{n}^{(A)} \right] \\
& \times H \left[\left(\frac{\mathbf{x}^C + \mathbf{x}^D + \mathbf{x}^A}{3} - \mathbf{x} \right) \cdot \mathbf{n}^{(B)} \right] \\
& \times H \left[\left(\frac{\mathbf{x}^D + \mathbf{x}^A + \mathbf{x}^B}{3} - \mathbf{x} \right) \cdot \mathbf{n}^{(C)} \right].
\end{aligned} \tag{55}$$

The stress field can then be obtained using (5), (6), (45), and (55).

The numerical solutions for the stress field based on the Gauss-Legendre and the double-exponential quadratures are compared in Figure 11 for the case of a tetrahedron with the vertices $A = (-5, -5, 5)$, $B = (-5, 5, 5)$, $C = (-5, 5, 15)$, and $D = (5, 5, 5)$ expressed in km and a non-trivial transformation strain ϵ_{11} of one microstrain. Using 15 integration points in each direction of integration with the Gauss-Legendre quadrature, some numerical artifacts scatter in the near-field, close to the surface of the tetrahedron. A close inspection of the residuals with analytic solutions shows that the numerical error decays away from the surface with a radial dependence. In the far-field, a low-order quadrature is sufficient to obtain double-precision accuracy, as noted by *Segall* (2010). In the near-field, the error can be eliminated with the double-exponential quadrature using more integration points. With 601 integration points in both directions of integration, the errors are less than can be represented with double-precision arithmetics.

Based on these results a simple heuristic can be devised to eliminate numerical errors and minimize the computational cost of these calculations whereby the double-exponential or the Gauss-Legendre quadrature is used depending on the distance from the center of the circumsphere. This approach guarantees double-precision accuracy with a computational cost comparable to using analytic solutions, all the while avoiding all possible numerical artifacts away from the surface of the tetrahedron. Some examples of stress interactions are shown in Figures 12 and 13 where the double-exponential quadrature was used for points within one radius from the circumsphere center.

Semi-analytic solution with a spectral method

I now derive numerical solutions compatible with the Fourier-domain semi-analytic solver of *Barbot and Fialko* (2010b) implemented in the software *Relax* that was recently optimized for parallel computing on GPU (*Masuti et al.*, 2014). The approach solves Navier's equation (3) analytically in the Fourier domain and provides the space-domain solution using a discrete Fourier transform. This approach is numerically more efficient than employing an analytic solution for large enough domains because of the scaling properties of the fast Fourier transform (e.g., *Liu and Wang*, 2005; *Liu et al.*, 2012). However, the

numerical accuracy is limited to about 1% due to undesirable periodic boundary conditions. At the heart of the method is the explicit sampling of the equivalent body-force density (11). This is obtained with

$$\begin{aligned}
-\nabla\Phi(\mathbf{x}) = & \mathbf{n}^{(D)} \delta \left[\left(\frac{\mathbf{x}^A + \mathbf{x}^B + \mathbf{x}^C}{3} - \mathbf{x} \right) \cdot \mathbf{n}^{(D)} \right] \cdot H \left[\left(\frac{\mathbf{x}^B + \mathbf{x}^C + \mathbf{x}^D}{3} - \mathbf{x} \right) \cdot \mathbf{n}^{(A)} \right] \\
& \cdot H \left[\left(\frac{\mathbf{x}^C + \mathbf{x}^D + \mathbf{x}^A}{3} - \mathbf{x} \right) \cdot \mathbf{n}^{(B)} \right] \cdot H \left[\left(\frac{\mathbf{x}^D + \mathbf{x}^A + \mathbf{x}^B}{3} - \mathbf{x} \right) \cdot \mathbf{n}^{(C)} \right] \\
+ & \mathbf{n}^{(A)} H \left[\left(\frac{\mathbf{x}^A + \mathbf{x}^B + \mathbf{x}^C}{3} - \mathbf{x} \right) \cdot \mathbf{n}^{(D)} \right] \cdot \delta \left[\left(\frac{\mathbf{x}^B + \mathbf{x}^C + \mathbf{x}^D}{3} - \mathbf{x} \right) \cdot \mathbf{n}^{(A)} \right] \\
& \cdot H \left[\left(\frac{\mathbf{x}^C + \mathbf{x}^D + \mathbf{x}^A}{3} - \mathbf{x} \right) \cdot \mathbf{n}^{(B)} \right] \cdot H \left[\left(\frac{\mathbf{x}^D + \mathbf{x}^A + \mathbf{x}^B}{3} - \mathbf{x} \right) \cdot \mathbf{n}^{(C)} \right] \\
+ & \mathbf{n}^{(B)} H \left[\left(\frac{\mathbf{x}^A + \mathbf{x}^B + \mathbf{x}^C}{3} - \mathbf{x} \right) \cdot \mathbf{n}^{(D)} \right] \cdot H \left[\left(\frac{\mathbf{x}^B + \mathbf{x}^C + \mathbf{x}^D}{3} - \mathbf{x} \right) \cdot \mathbf{n}^{(A)} \right] \\
& \cdot \delta \left[\left(\frac{\mathbf{x}^C + \mathbf{x}^D + \mathbf{x}^A}{3} - \mathbf{x} \right) \cdot \mathbf{n}^{(B)} \right] \cdot H \left[\left(\frac{\mathbf{x}^D + \mathbf{x}^A + \mathbf{x}^B}{3} - \mathbf{x} \right) \cdot \mathbf{n}^{(C)} \right] \\
+ & \mathbf{n}^{(C)} H \left[\left(\frac{\mathbf{x}^A + \mathbf{x}^B + \mathbf{x}^C}{3} - \mathbf{x} \right) \cdot \mathbf{n}^{(D)} \right] \cdot H \left[\left(\frac{\mathbf{x}^B + \mathbf{x}^C + \mathbf{x}^D}{3} - \mathbf{x} \right) \cdot \mathbf{n}^{(A)} \right] \\
& \cdot H \left[\left(\frac{\mathbf{x}^C + \mathbf{x}^D + \mathbf{x}^A}{3} - \mathbf{x} \right) \cdot \mathbf{n}^{(B)} \right] \cdot \delta \left[\left(\frac{\mathbf{x}^D + \mathbf{x}^A + \mathbf{x}^B}{3} - \mathbf{x} \right) \cdot \mathbf{n}^{(C)} \right].
\end{aligned} \tag{56}$$

For the stability of the Fourier transform and to avoid Gibbs oscillations near sharp discontinuities, the Heaviside function is replaced with an error function

$$H(x) \sim \frac{1}{2} \left[1 + \operatorname{erf} \left(\frac{x}{\sigma\sqrt{2}} \right) \right] \tag{57}$$

and the Delta function is replaced with a Gaussian function

$$\delta(x) \sim \frac{1}{\sqrt{2\pi}\sigma^2} \exp \left(-\frac{x^2}{2\sigma^2} \right) \tag{58}$$

Both approximations are exact in the limit $\sigma \rightarrow 0$ and in practice I employ $\sigma = \Delta x$, using the numerical sampling size as a smoothing factor. This choice is appropriate to conserve linear momentum, i.e., (58) is the derivative of (57), and to suppress singular points near the vertices of the tetrahedron. Figure 14 shows the displacement field and the pressure field induced by an isotropic transformation strain, which may find some applications in hydrological studies. The isotropic strain does not impact a change of pressure in the surrounding medium except near the free surface, as remarked earlier (*Barbot et al., 2017; Faivre, 1969*). This observation also serves as a sophisticated benchmark.

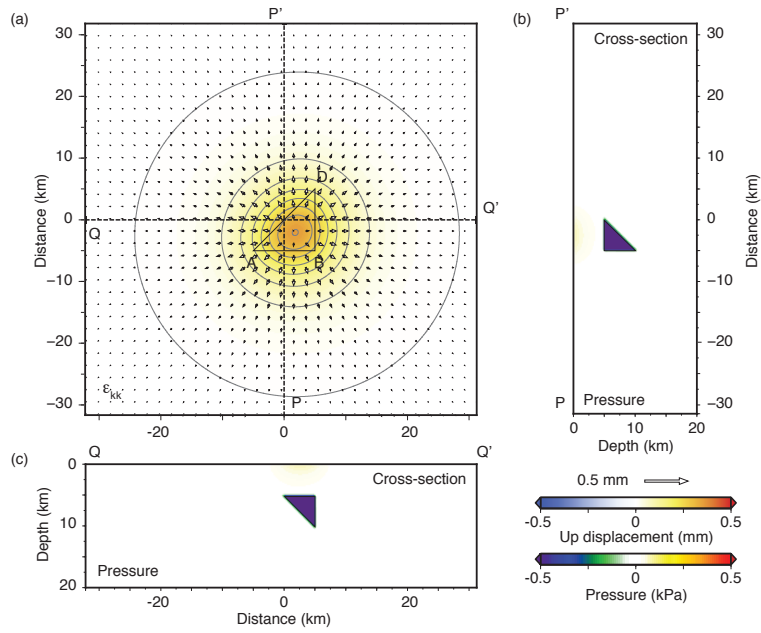


Figure 14: Displacement at the surface and pressure in the half-space due to isotropic transformation strain confined in a tetrahedral volume ABCD calculated with a spectral method. A) The arrows indicate horizontal displacements and the background indicates the vertical (positive up) displacement. B) The pressure field in the cross-section P-P'. C) The pressure in the cross-section Q-Q'. The transformation strain is $\epsilon_{11} = \epsilon_{22} = \epsilon_{33} = 0.33 \times 10^{-6}$. The vertical displacement contours are every 0.05 mm.

Conclusions

I have presented solutions for the displacement and stress kernels in a half-space associated with transformation strain confined in a tetrahedral volume. Numerical and analytic solutions provide the same accuracy, can be evaluated with commensurate computational costs, but numerical quadratures can be more stable in some cases. This work may afford more accurate models of distributed deformation that incorporate structural data. While I hope these results will be useful, some key elements are missing, such as the stratification of elastic properties, surface topography (e.g., *Cayol and Cornet*, 1997; *Mayo*, 1985; *McKenney et al.*, 1995; *McTigue and Segall*, 1988; *Wang et al.*, 2018; *Williams and Wadge*, 1998, 2000), in particular, Earth’s curvature (*Pollitz*, 1997; *Yu and Okubo*, 2016), and coupling with gravity (*Okubo*, 1992; *Rundle*, 1982; *Wang et al.*, 2006). For more realistic models with lateral variations of elastic moduli, fully numerical methods may be employed (e.g., *Landry and Barbot*, 2016, 2018).

Acknowledgements

The author gratefully acknowledges the thoughtful comments of three anonymous reviewers. This research was supported by the National Research Foundation of Singapore under the NRF Fellowship scheme (National Research Fellow Awards No. NRF-NRFF2013-04) and by the Earth Observatory of Singapore, the National Research Foundation, and the Singapore Ministry of Education under the Research Centres of Excellence initiative.

Data and Resources

The MATLAB computer programs used in the manuscript are available at <https://bitbucket.org/sbarbot> (last accessed in June 2018). The *Relax* modeling software is hosted at www.geodynamics.org (last accessed in February 2018) with support from the Computational Infrastructure for Geodynamics.

References

- Aagaard, B. T., M. G. Knepley, and C. A. Williams, A domain decomposition approach to implementing fault slip in finite-element models of quasi-static and dynamic crustal deformation, *J. Geophys. Res.*, 118(6), 3059–3079, 2013.
- Abramowitz, M., and I. Stegun, *Handbook of mathematical functions with formulas, graphs and mathematical tables*, 1046 pp., U.S. Govt. Print. Off., Washington DC, 1972.
- Andrews, D., Coupling of energy between tectonic processes and earthquakes, *J. Geophys. Res.*, 83(B5), 2259–2264, 1978.

- Barbot, S., Asthenosphere flow modulated by megathrust earthquake cycles, *submitted to Geophys. Res. Lett.*, doi:10.17605/OSF.IO/G8AHE, 2018.
- Barbot, S., and Y. Fialko, A unified continuum representation of postseismic relaxation mechanisms: semi-analytic models of afterslip, poroelastic rebound and viscoelastic flow, *Geophys. J. Int.*, *182*(3), 1124–1140, doi:10.1111/j.1365-246X.2010.04678.x, 2010a.
- Barbot, S., and Y. Fialko, Fourier-domain Green’s function for an elastic semi-infinite solid under gravity, with applications to earthquake and volcano deformation, *Geophys. J. Int.*, *182*(2), 568–582, doi:10.1111/j.1365-246X.2010.04655.x, 2010b.
- Barbot, S., Y. Fialko, and D. Sandwell, Effect of a compliant fault zone on the inferred earthquake slip distribution, *J. Geophys. Res.*, *113*(B6), doi: 10.1029/2007JB005256, 2008.
- Barbot, S., J. D. Moore, and V. Lambert, Displacement and stress associated with distributed anelastic deformation in a half-space, *Bull. Seism. Soc. Am.*, *107*(2), 821–855, 2017.
- Barnhart, W. D., and R. B. Lohman, Automated fault model discretization for inversions for coseismic slip distributions, *J. Geophys. Res.*, *115*(B10419), 17 PP., 2010.
- Beer, G., I. Smith, and C. Duenser, *The boundary element method with programming: for engineers and scientists*, Springer Science & Business Media, 2008.
- Biemiller, J., and L. Lavier, Earthquake supercycles as part of a spectrum of normal fault slip styles, *Journal of Geophysical Research: Solid Earth*, *122*(4), 3221–3240, 2017.
- Cayol, V., and F. Cornet, 3d mixed boundary elements for elastostatic deformation field analysis, *International journal of rock mechanics and mining sciences*, *34*(2), 275–287, 1997.
- Chinnery, M., The stress changes that accompany strike-slip faulting, *Bull. Seism. Soc. Am.*, *53*(5), 921–932, 1963.
- Chiu, Y., On the stress field and surface deformation in a half space with a cuboidal zone in which initial strains are uniform, *Journal of Applied Mechanics*, *45*(2), 302–306, 1978.
- Cohen, S. C., Convenient formulas for determining dip-slip fault parameters from geophysical observables, *Bull. Seism. Soc. Am.*, *86*(5), 1642–1644, 1996.
- Comninou, M., and J. Dundurs, The angular dislocation in a half space, *Journal of Elasticity*, *5*(3-4), 203–216, 1975.

- Daout, S., S. Barbot, G. Peltzer, M.-P. Doin, Z. Liu, and R. Jolivet, Constraining the kinematics of metropolitan los angeles faults with a slip-partitioning model, *Geophys. Res. Lett.*, *43*(21), 2016a.
- Daout, S., R. Jolivet, C. Lasserre, M.-P. Doin, S. Barbot, P. Tapponnier, G. Peltzer, A. Socquet, and J. Sun, Along-strike variations of the partitioning of convergence across the haiyuan fault system detected by insar, *Geophys. J. Int.*, *205*(1), 536–547, 2016b.
- Dieterich, J. H., and K. B. Richards-Dinger, Earthquake recurrence in simulated fault systems, *Pure Appl. Geophys.*, *167*(8-9), 1087–1104, 2010.
- Dinther, Y. v., T. V. Gerya, L. A. Dalguer, P. M. Mai, G. Morra, and D. Giardini, The seismic cycle at subduction thrusts: Insights from seismo-thermo-mechanical models, *J. Geophys. Res.*, *118*(12), 6183–6202, 2013.
- Dundurs, J., Force in smoothly joined elastic half-planes, *Journal of the Engineering Mechanics Division*, *88*(5), 25–66, 1962.
- Erickson, B. A., E. M. Dunham, and A. Khosravifar, A finite difference method for off-fault plasticity throughout the earthquake cycle, *Journal of the Mechanics and Physics of Solids*, *109*, 50–77, 2017.
- Faivre, G., Deformations de coherence d'un precipite quadratique, *physica status solidi (b)*, *35*(1), 249–259, 1969.
- Furuya, M., and T. Yasuda, The 2008 yutian normal faulting earthquake (mw 7.1), nw tibet: Non-planar fault modeling and implications for the karakax fault, *Tectonophysics*, *511*(3-4), 125–133, 2011.
- Glas, F., Coherent stress relaxation in a half space: modulated layers, inclusions, steps, and a general solution, *Journal of applied physics*, *70*(7), 3556–3571, 1991.
- Golub, G. H., and J. H. Welsch, Calculation of gauss quadrature rules, *Mathematics of computation*, *23*(106), 221–230, 1969.
- Gosling, T., and J. Willis, A line-integral representation for the stresses due to an arbitrary dislocation in an isotropic half-space, *J. Mech. Phys. Solids*, *42*(8), 1199–1221, 1994.
- Goswami, A., and S. Barbot, Slow-slip events in semi-brittle serpentinite fault zones, *Scientific reports*, *8*(1), 6181, 2018.
- Govers, R., K. Furlong, L. Wiel, M. Herman, and T. Broerse, The geodetic signature of the earthquake cycle at subduction zones: Model constraints on the deep processes, *Reviews of Geophysics*, 2017.
- Haber, S., The tanh rule for numerical integration, *SIAM J. Numerical Analysis*, *14*(4), 668–685, 1977.

- Hirahara, K., Interplate earthquake fault slip during periodic earthquake cycles in a viscoelastic medium at a subduction zone, *Pure and applied geophysics*, *159*(10), 2201–2220, 2002.
- Iwasaki, T., and R. Sato, Strain field in a semi-infinite medium due to an inclined rectangular fault., *J. Phys. Earth*, *27*(4), 285–314, 1979.
- Jeyakumaran, M., J. Rudnicki, and L. Keer, Modeling slip zones with triangular dislocation elements, *Bull. Seism. Soc. Am.*, *82*(5), 2153–2169, 1992.
- Lambert, V., and S. Barbot, Contribution of viscoelastic flow in earthquake cycles within the lithosphere-asthenosphere system, *Geophys. Res. Lett.*, *43*(19), 142–154, 2016.
- Landry, W., and S. Barbot, Gamra: Simple meshing for complex earthquakes, *Computers and Geosciences*, *90*, 49–63, doi:10.1016/j.cageo.2016.02.014, 2016.
- Landry, W., and S. Barbot, Fast, accurate solutions for curvilinear earthquake faults and anelastic strain, *arXiv preprint arXiv:1802.08931*, 2018.
- Li, D., and Y. Liu, Spatiotemporal evolution of slow slip events in a nonplanar fault model for northern cascadia subduction zone, *J. Geophys. Res.*, *121*(9), 6828–6845, 2016.
- Lindsey, E. O., V. J. Sahakian, Y. Fialko, Y. Bock, S. Barbot, and T. K. Rockwell, Interseismic strain localization in the san jacinto fault zone, *Pure and Applied Geophysics*, *171*(11), 2937–2954, 2014.
- Liu, S., and Q. Wang, Elastic fields due to eigenstrains in a half-space, *Journal of applied mechanics*, *72*(6), 871–878, 2005.
- Liu, S., X. Jin, Z. Wang, L. M. Keer, and Q. Wang, Analytical solution for elastic fields caused by eigenstrains in a half-space and numerical implementation based on fft, *International Journal of Plasticity*, *35*, 135–154, 2012.
- Liu, Y., and J. R. Rice, Aseismic slip transients emerge spontaneously in three-dimensional rate and state modeling of subduction earthquake sequences, *J. Geophys. Res.*, *110*(B08307), doi:10.1029/2004JB003424, 2005.
- Maerten, F., P. Resor, D. Pollard, and L. Maerten, Inverting for slip on three-dimensional fault surfaces using angular dislocations, *Bull. Seism. Soc. Am.*, *95*(5), 1654–1665, 2005.
- Mansinha, L., and D. Smylie, The displacement fields of inclined faults, *Bull. Seism. Soc. Am.*, *61*(5), 1433–1440, 1971.
- Marshall, S. T., M. L. Cooke, and S. E. Owen, Interseismic deformation associated with three-dimensional faults in the greater los angeles region, california, *J. Geophys. Res.*, *114*(B12), 2009.

- Masuti, S. S., S. Barbot, and N. Kapre, Relax-miracle: Gpu parallelization of semi-analytic fourier-domain solvers for earthquake modeling, in *High Performance Computing (HiPC), 2014 21st International Conference on*, pp. 1–10, IEEE, 2014.
- Mayo, A., Fast high order accurate solution of laplace's equation on irregular regions, *SIAM journal on scientific and statistical computing*, 6(1), 144–157, 1985.
- McKenney, A., L. Greengard, and A. Mayo, A fast poisson solver for complex geometries, *Journal of Computational Physics*, 118(2), 348–355, 1995.
- McTigue, D. F., and P. Segall, Displacements and tilts from dip-slip faults and magma chambers beneath irregular surface topography, *J. Geophys. Res.*, 15(6), 601–604, 1988.
- Meade, B. J., Algorithms for the calculation of exact displacements, strains, and stresses for triangular dislocation elements in a uniform elastic half space, *Comp. Geosc.*, 33(8), 1064–1075, 2007.
- Melan, E., Der spannungszustand der durch eine einzelkraft im innern beanspruchten halbscheibe, *ZAMM-Journal of Applied Mathematics and Mechanics/Zeitschrift für Angewandte Mathematik und Mechanik*, 12(6), 343–346, 1932.
- Mindlin, R. D., Force at a point in the interior of a semi-infinite solid, *J. Appl. Phys.*, 7, 195–202, 1936.
- Moore, J. D., Yu H., Tang C.-H., Wang T., Barbot S., Peng D., Masuti S., Dauwels J., Hsu Y.-J., Lambert V., et al., Imaging the distribution of transient viscosity after the 2016 mw 7.1 kumamoto earthquake, *Science*, 356(6334), 163–167, 2017.
- Murray, J., and J. Langbein, Slip on the San Andreas Fault at Parkfield, California, over Two Earthquake Cycles, and the Implications for Seismic Hazard, *Bull. Seism. Soc. Am.*, 96(4B), S283–S303, 2006.
- Muto, J., B. Shibazaki, Y. Ito, T. Inuma, M. Ohzono, T. Matsumoto, and T. Okada, Two-dimensional viscosity structure of the northeastern japan islands arc-trench system, *Geophys. Res. Lett.*, 40(17), 4604–4608, 2013.
- Muto, J., B. Shibazaki, T. Inuma, Y. Ito, Y. Ohta, S. Miura, and Y. Nakai, Heterogeneous rheology controlled postseismic deformation of the 2011 tohoku-oki earthquake, *Geophys. Res. Lett.*, 43(10), 4971–4978, 2016.
- Nikkhoo, M., and T. R. Walter, Triangular dislocation: an analytical, artefact-free solution, *Geophys. J. Int.*, 201(2), 1117–1139, 2015.
- Nozaki, H., and M. Taya, Elastic fields in a polygon-shaped inclusion with uniform eigenstrains, *Journal of applied mechanics*, 64(3), 495–502, 1997.

- Nozaki, H., and M. Taya, Elastic fields in a polyhedral inclusion with uniform eigenstrains and related problems, *Journal of Applied mechanics*, 68(3), 441–452, 2001.
- Nur, A., and M. Israel, The role of heterogeneities in faulting, *Physics of the Earth and Planetary Interiors*, 21(2-3), 225–236, 1980.
- Nur, A., and G. Mavko, Postseismic viscoelastic rebound, *Science*, 183, 204–206, 1974.
- Ohtani, M., and K. Hirahara, Effect of the earth’s surface topography on quasi-dynamic earthquake cycles, *Geophys. J. Int.*, 203(1), 384–398, 2015.
- Okada, Y., Surface deformation due to shear and tensile faults in a half-space, *Bull. Seism. Soc. Am.*, 75(4), 1135–1154, 1985.
- Okada, Y., Internal deformation due to shear and tensile faults in a half-space, *Bull. Seism. Soc. Am.*, 82, 1018–1040, 1992.
- Okubo, S., Gravity and potential changes due to shear and tensile faults in a half-space, *J. Geophys. Res.*, 97(B5), 7137–7144, 1992.
- Pollitz, F. F., Gravitational viscoelastic postseismic relaxation on a layered spherical Earth, *J. Geophys. Res.*, 102, 17,921–17,941, 1997.
- Pozrikidis, C., *A practical guide to boundary element methods with the software library BEMLIB*, CRC Press, 2002.
- Press, F., Displacements, strains, and tilts at teleseismic distances, *J. Geophys. Res.*, 70(10), 2395–2412, 1965.
- Qiu, Q., J. D. P. Moore, S. Barbot, L. Feng, and E. Hill, Transient viscosity in the Sumatran mantle wedge from a decade of geodetic observations, *Nature Communications*, 2018.
- Qiu, Q., Hill E. M., Barbot S., Hubbard J., Feng W., Lindsey E.O., Feng L., Dai K., Samsonov S. V., Tapponnier P., The mechanism of partial rupture of a locked megathrust: The role of fault morphology, *Geology*, 44(10), 875–878, 2016.
- Romanet, P., H. S. Bhat, R. Jolivet, and R. Madariaga, Fast and slow slip events emerge due to fault geometrical complexity, *Geophys. Res. Lett.*, 2018.
- Rundle, J. B., Viscoelastic-gravitational deformation by a rectangular thrust fault in a layered earth, *J. Geophys. Res.*, 87(B9), 7787–7796, 1982.
- Sato, R., and M. Matsu’ura, Strains and tilts on the surface of a semi-infinite medium, *J. Phys. Earth*, 22(2), 213–221, 1974.
- Savage, J., A dislocation model of strain accumulation and release at a subduction zone, *J. Geophys. Res.*, 88(B6), 4984–4996, 1983.

- Savage, J. C., Displacement field for an edge dislocation in a layered half-space, *J. Geophys. Res.*, 103(B2), 2439–2446, 1998.
- Savage, J. C., and L. M. Hastie, Surface deformation associated with dip-slip faulting, *J. Geophys. Res.*, 71(20), 4897–4904, 1966.
- Savage, J. C., and W. H. Prescott, Asthenosphere readjustment and the earthquake cycle, *J. Geophys. Res.*, 83(B7), 3369–3376, 1978.
- Segall, P., *Earthquake and volcano deformation*, Princeton University Press, Princeton, NJ, 2010.
- Steer, P., M. Simoes, R. Cattin, and J. B. H. Shyu, Erosion influences the seismicity of active thrust faults, *Nature communications*, 5, 5564, 2014.
- Steketee, J. A., Some geophysical applications of the elasticity theory of dislocations, *Can. J. Phys.*, 36, 1168–1198, 1958.
- Takeuchi, C. S., and Y. Fialko, On the effects of thermally weakened ductile shear zones on postseismic deformation, *J. Geophys. Res.*, 118(12), 6295–6310, 2013.
- Thatcher, W., and J. R. Rundle, A model for the earthquake cycle in underthrust zones, *J. Geophys. Res.*, 84(B10), 5540–5556, 1979.
- Tsang, L. L. H., E. M. Hill, S. Barbot, Q. Qiu, L. Feng, I. Hermawan, P. Banerjee, and D. H. Natawidjaja, PCAIM models of postseismic deformation with afterslip and viscoelastic deformation following the 2007 Mw 8.6 Bengkulu earthquake, *J. Geophys. Res.*, 2016.
- Walter, T. R., and F. Amelung, Volcano-earthquake interaction at mauna loa volcano, hawaii, *J. Geophys. Res.*, 111(B5), 2006.
- Wang, R., F. Martin, and F. Roth, Computation of deformation induced by earthquakes in a multi-layered elastic crust - FORTRAN programs ED-GRN/EDCMP, *Comp. Geosci.*, 29, 195–207, 2003.
- Wang, R., F. Lorenzo-Martin, and F. Roth, PSGRN/PSCMP-a new code for calculating co- and post-seismic deformation, geoid and gravity changes based on the viscoelastic-gravitational dislocation theory, *Computers and Geosciences*, 32, 527–541, 2006.
- Wang, T., Q. Shi, M. Nikkhoo, S. Wei, S. Barbot, D. Dreger, R. Bürgmann, M. Motagh, and Q.-F. Chen, The rise, collapse, and compaction of mt. mantap from the 3 september 2017 north korean nuclear test, *Science*, p. eaar7230, 2018.
- Williams, C. A., and G. Wadge, The effects of topography on magma chamber deformation models: Application to mt. etna and radar interferometry, *Geophys. Res. Lett.*, 25(10), 1549–1552, 1998.

- Williams, C. A., and G. Wadge, An accurate and efficient method for including the effects of topography in three-dimensional elastic models of ground deformation with applications to radar interferometry, *J. Geophys. Res.*, 105(B4), 8103–8120, 2000.
- Yoffe, E. H., The angular dislocation, *Philosophical Magazine*, 5(50), 161–175, 1960.
- Yu, T., and S. Okubo, Internal deformation caused by a point dislocation in a uniform elastic sphere, *Geophys. J. Int.*, 208(2), 973–991, 2016.

Appendix A. Analytic solution for line integrals of the half-space elasto-static Green's function in plane strain

The closed-form solutions for the line integral (29) of the half-space Green's functions can be obtained using symbolic algebra with *Maple*[®]. The displacement field only depends on the coordinates of the end-points of the line integral, so that

$$U_{ij} = \int_{AB} G_{ij}(x_2, x_3; y_2, y_3) dy_2 dy_3 = I_{ij} \left(\frac{R}{2} \right) - I_{ij} \left(-\frac{R}{2} \right), \quad (\text{A1})$$

for $i, j = 2, 3$, where R is the length of segment AB. For increased clarity, I define the mid-point coordinates

$$\mathbf{m} = \frac{\mathbf{x}^A + \mathbf{x}^B}{2} \quad (\text{A2})$$

and the azimuthal vector

$$\mathbf{a} = \frac{\mathbf{x}^B - \mathbf{x}^A}{\|AB\|} \quad (\text{A3})$$

The expressions for $I_{ij}(t)$ are provided below.

$$\begin{aligned} I_{22}(t) = & \frac{-1}{2\pi(-1+\nu)} \left\{ \left(\frac{1}{2} t(-3/4+\nu) a_2^4 + 1/2 (-3/4+\nu) (-x_2+m_2) a_2^3 \right. \right. \\ & - 1/2 (-2t(-3/4+\nu) a_3 + (\nu-5/4)(x_3-m_3)) a_3 a_2^2 \\ & + 1/2 (-1/4+\nu) a_3^2 (-x_2+m_2) a_2 - 1/2 (x_3-m_3-a_3 t) a_3^3 (-3/4+\nu) \Big) \\ & \cdot \ln \left[t^2 + ((2m_2-2x_2)a_2 + 2a_3(-x_3+m_3))t + (x_2-m_2)^2 + (x_3-m_3)^2 \right] \\ & + ((x_3-m_3)a_2 + a_3(-x_2+m_2))((-1+\nu)a_2^2 + (-1/2+\nu)a_3^2) \\ & \cdot \arctan \left[\frac{-ta_2^2 + (-m_2+x_2)a_2 - a_3(a_3 t - x_3 + m_3)}{(-x_3+m_3)a_2 - a_3(-x_2+m_2)} \right] \\ & \left. - ((-3/4+\nu)a_2^2 + (-1/2+\nu)a_3^2)t \right\} \\ & + \frac{5-12\nu+8\nu^2}{8\pi(-1+\nu)} \left\{ (1/2 ta_2^2 + (1/2 m_2 - 1/2 x_2) a_2 + 1/2 a_3 (x_3 + m_3 + a_3 t)) \right. \\ & \cdot \ln \left[t^2 + ((2m_2-2x_2)a_2 + 2a_3(x_3+m_3))t + (x_2-m_2)^2 + (x_3+m_3)^2 \right] \\ & + ((x_3+m_3)a_2 - a_3(-x_2+m_2)) \\ & \left. \cdot \arctan \left[\frac{ta_2^2 + (-x_2+m_2)a_2 + a_3(x_3+m_3+a_3 t)}{(x_3+m_3)a_2 - a_3(-x_2+m_2)} \right] - t \right\} \end{aligned}$$

$$\begin{aligned}
& + \frac{1}{8\pi(-1+\nu)} \left[-4 \left(((x_3+m_3)\nu - x_3 - 3/4 m_3) a_2^2 \right. \right. \\
& \quad \left. \left. - (-3/4 + \nu) a_3 (-x_2 + m_2) a_2 - 1/4 a_3^2 x_3 \right) (a_3 (-m_2 + x_2) + (x_3 + m_3) a_2) a_3 \right. \\
& \quad \cdot \ln \left[t^2 + ((2m_2 - 2x_2) a_2 + 2a_3 (x_3 + m_3)) t + (x_2 - m_2)^2 + (x_3 + m_3)^2 \right] \\
& \quad + \left\{ (4(-x_2 + m_2)^2 \nu - 2x_3^2 - 3(-x_2 + m_2)^2) a_3^4 \right. \\
& \quad \left. - 8a_3^3 ((x_3 + m_3)\nu - 3/4 m_3 - 1/2 x_3) (-x_2 + m_2) a_2 \right. \\
& \quad \left. + 4 \left((m_2 + x_3 + m_3 - x_2) (-m_2 + x_3 + m_3 + x_2) \nu \right. \right. \\
& \quad \quad \left. \left. - 5/4 x_3^2 - x_3 m_3 + 3/4 (m_2 - m_3 - x_2) (m_2 + m_3 - x_2) \right) a_3^2 a_2^2 \right. \\
& \quad \left. + 8a_3 (-x_2 + m_2) ((x_3 + m_3)\nu - x_3 - 3/4 m_3) a_2^3 \right. \\
& \quad \left. - 4 \left((x_3 + m_3)^2 \nu - 3/4 m_3^2 - 2x_3 m_3 - 3/4 x_3^2 \right) a_2^4 \right\} \\
& \quad \cdot \arctan \left(\frac{t a_2^2 + (-x_2 + m_2) a_2 + a_3 (x_3 + m_3 + a_3 t)}{(x_3 + m_3) a_2 - a_3 (-x_2 + m_2)} \right) \\
& \quad \left. - 4t (a_2^2 + a_3^2) (-3/4 + \nu) (a_3 (-m_2 + x_2) + (x_3 + m_3) a_2) a_3^2 \right] \\
& \quad / \left(a_3 (-m_2 + x_2) + (x_3 + m_3) a_2 \right) \\
& - \frac{x_3}{4\pi(-1+\nu)} \left\{ (a_3 (-m_2 + x_2) + (x_3 + m_3) a_2) a_3^3 \left(a_3^2 t^2 + 2t (x_3 + m_3) a_3 \right. \right. \\
& \quad \left. \left. + a_2^2 t^2 + 2t (-x_2 + m_2) a_2 + (x_3 + m_3)^2 + (x_2 - m_2)^2 \right) \right. \\
& \quad \cdot \ln \left[t^2 + 2((m_2 - x_2) a_2 + a_3 (x_3 + m_3)) t + (x_2 - m_2)^2 + (x_3 + m_3)^2 \right] \\
& \quad + \left(-a_3^4 x_3 - 3(-x_2 + m_2) a_2 a_3^3 + a_2^2 (3m_3 + x_3) a_3^2 \right. \\
& \quad \quad \left. - a_2^3 (-x_2 + m_2) a_3 + m_3 a_2^4 \right) \\
& \quad \cdot (a_3^2 t^2 + 2t (x_3 + m_3) a_3 + a_2^2 t^2 \\
& \quad \quad + 2t (-x_2 + m_2) a_2 + (x_3 + m_3)^2 + (x_2 - m_2)^2) \\
& \quad \cdot \arctan \left[\frac{t a_2^2 + (-x_2 + m_2) a_2 + a_3 (x_3 + m_3 + a_3 t)}{(x_3 + m_3) a_2 - a_3 (-x_2 + m_2)} \right] \\
& \quad \left. - \left(-t a_3^4 x_3 + \left(-3t (-x_2 + m_2) a_2 - x_3^2 - x_3 m_3 - (-x_2 + m_2)^2 \right) a_3^3 \right. \right. \\
& \quad \left. \left. + 3a_2 (t (x_3 + m_3) a_2 - 1/3 m_3 (-x_2 + m_2)) a_3^2 \right) \right\}
\end{aligned}$$

$$\begin{aligned}
& + a_3 a_2^2 \left(t(-x_2 + m_2) a_2 + x_3^2 + 3 x_3 m_3 + 2 m_3^2 + (-x_2 + m_2)^2 \right) \\
& - m_3 a_2^3 (-x_2 + m_2 + a_2 t) \left(a_3 (-m_2 + x_2) + (x_3 + m_3) a_2 \right) \Big\} \\
& (a_3 (-m_2 + x_2) + (x_3 + m_3) a_2)^{-1} \left((x_3 + m_3 + a_3 t)^2 + (x_2 - m_2 - a_2 t)^2 \right)^{-1} \\
I_{23}(t) = & \frac{1}{4\pi(-1+\nu)} \left\{ \frac{1}{4} \left((x_3 - m_3) a_2 - a_3 (x_2 - m_2) \right) (a_2 - a_3) (a_2 + a_3) \right. \\
& \cdot \ln \left(t^2 + ((2m_2 - 2x_2) a_2 + 2a_3 (-x_3 + m_3)) t + (x_2 - m_2)^2 + (x_3 - m_3)^2 \right) \\
& + a_2 a_3 \left((x_3 - m_3) a_2 + a_3 (-x_2 + m_2) \right) \\
& \left. \cdot \arctan \left(\frac{-ta_2^2 + (-m_2 + x_2) a_2 - a_3 (a_3 t - x_3 + m_3)}{(-x_3 + m_3) a_2 - a_3 (x_2 + m_2)} \right) - 1/2 t \right\} \\
& + \frac{1}{a_3 \pi (-1/2 + \nu)} \left\{ -\frac{1}{2} (a_3 (-m_2 + x_2) + (x_3 + m_3) a_2) a_3 \right. \\
& \cdot \ln \left[\left(-\frac{a_2}{a_3} + \frac{a_2 x_3 + a_2 m_3 + a_3 x_2 - a_3 m_2}{a_3 (x_3 + m_3 + a_3 t)} \right)^2 + 1 \right] \\
& - (a_3 (-m_2 + x_2) + (x_3 + m_3) a_2) a_2 \\
& \cdot \arctan \left[\frac{ta_2^2 + (-x_2 + m_2) a_2 + a_3 (x_3 + m_3 + a_3 t)}{(x_3 + m_3) a_2 - a_3 (-x_2 + m_2)} \right] \\
& + (a_3 (-m_2 + x_2) + (x_3 + m_3) a_2) a_3 \ln \left[\frac{a_3 (-m_2 + x_2) + (x_3 + m_3) a_2}{x_3 + m_3 + a_3 t} \right] \\
& + (a_3 (-m_2 + x_2) + (x_3 + m_3) a_2) a_2 \arctan \left(\frac{a_3}{a_2} \right) \\
& \left. + (x_3 + m_3 + a_3 t) \arctan \left(\frac{-x_2 + m_2 + a_2 t}{x_3 + m_3 + a_3 t} \right) \right\} \\
& + \frac{-3 + 4\nu}{4\pi(-1+\nu)} \left\{ \left((-1/4 x_2 + 1/4 m_2) a_3^3 - 3/4 (x_3 + 1/3 m_3) a_2 a_3^2 \right. \right. \\
& \left. \left. - 1/4 a_2^2 (-x_2 + m_2) a_3 - 1/4 a_2^3 (x_3 - m_3) \right) \right. \\
& \cdot \ln \left[t^2 + ((2m_2 - 2x_2) a_2 + 2a_3 (x_3 + m_3)) t + (x_2 - m_2)^2 + (x_3 - m_3)^2 \right] \\
& + \left((a_3^2 x_3 + (-x_2 + m_2) a_2 a_3 - a_2^2 m_3) \right. \\
& \left. \cdot \arctan \left[\frac{ta_2^2 + (-x_2 + m_2) a_2 + a_3 (x_3 + m_3 + a_3 t)}{(x_3 + m_3) a_2 - a_3 (-x_2 + m_2)} \right] + 1/2 a_2 t \right) a_3 \Big\} \\
& - \frac{1}{4\pi(-1+\nu)} x_3 \left\{ a_2 \left(a_3^2 t^2 + 2t(x_3 + m_3) a_3 + a_2^2 t^2 + 2t(-x_2 + m_2) a_2 \right. \right.
\end{aligned}$$

$$\begin{aligned}
& + m_3^2 + 2x_3 m_3 + x_3^2 + (-x_2 + m_2)^2 \Big) a_3^2 \\
& \cdot \ln \left[t^2 + ((2m_2 - 2x_2)a_2 + 2a_3(x_3 + m_3))t + (x_2 - m_2)^2 + (x_3 + m_3)^2 \right] \\
& + a_3(a_2 - a_3)(a_2 + a_3) \left(a_3^2 t^2 + 2t(x_3 + m_3)a_3 + a_2^2 t^2 \right. \\
& \quad \left. + 2t(-x_2 + m_2)a_2 + m_3^2 + 2x_3 m_3 + x_3^2 + (-x_2 + m_2)^2 \right) \\
& \cdot \arctan \left[\frac{ta_2^2 + (-x_2 + m_2)a_2 + a_3(x_3 + m_3 + a_3 t)}{(x_3 + m_3)a_2 - a_3(-x_2 + m_2)} \right] \\
& - t(-x_2 + m_2)a_3^4 + (3t(x_3 + 1/3 m_3)a_2 - m_3(-x_2 + m_2))a_3^3 \\
& \quad + 2a_2 \left(3/2 t(-x_2 + m_2)a_2 + 1/2 m_3^2 + 3/2 x_3 m_3 + x_3^2 + (-x_2 + m_2)^2 \right) a_3^2 \\
& \quad - a_2^2 \left(t(3m_3 + x_3)a_2 + m_3(-x_2 + m_2) \right) a_3 - m_3 a_2^3 (x_3 + m_3) \Big\} \\
& \quad \Big/ \left((x_3 + m_3 + a_3 t)^2 + (x_2 - m_2 - a_2 t)^2 \right) \\
I_{32}(t) = & \frac{1}{4\pi(-1 + \nu)} \left\{ \frac{1}{4} \left((x_3 - m_3)a_2 - a_3(x_2 - m_2) \right) (a_2 - a_3)(a_2 + a_3) \right. \\
& \cdot \ln \left(t^2 + ((2m_2 - 2x_2)a_2 + 2a_3(-x_3 + m_3))t + (x_2 - m_2)^2 + (x_3 - m_3)^2 \right) \\
& + a_2 a_3 \left(\left((x_3 - m_3)a_2 + a_3(-x_2 + m_2) \right) \right. \\
& \quad \left. \cdot \arctan \left(\frac{-ta_2^2 + (-m_2 + x_2)a_2 - a_3(a_3 t - x_3 + m_3)}{(-x_3 + m_3)a_2 - a_3(x_2 + m_2)} \right) - 1/2 t \right) \Big\} \\
& + \frac{1}{a_3 \pi(-1/2 + \nu)} \left\{ -\frac{1}{2} \left(a_3(-m_2 + x_2) + (x_3 + m_3)a_2 \right) a_3 \right. \\
& \cdot \ln \left[\left(-\frac{a_2}{a_3} + \frac{a_2 x_3 + a_2 m_3 + a_3 x_2 - a_3 m_2}{a_3(x_3 + m_3 + a_3 t)} \right)^2 + 1 \right] \\
& - \left(a_3(-m_2 + x_2) + (x_3 + m_3)a_2 \right) a_2 \\
& \cdot \arctan \left[\frac{ta_2^2 + (-x_2 + m_2)a_2 + a_3(x_3 + m_3 + a_3 t)}{(x_3 + m_3)a_2 - a_3(-x_2 + m_2)} \right] \\
& + \left(a_3(-m_2 + x_2) + (x_3 + m_3)a_2 \right) a_3 \ln \left[\frac{a_3(-m_2 + x_2) + (x_3 + m_3)a_2}{x_3 + m_3 + a_3 t} \right] \\
& + \left(a_3(-m_2 + x_2) + (x_3 + m_3)a_2 \right) a_2 \arctan \left(\frac{a_3}{a_2} \right) \\
& \left. + (x_3 + m_3 + a_3 t) \arctan \left(\frac{-x_2 + m_2 + a_2 t}{x_3 + m_3 + a_3 t} \right) \right\}
\end{aligned}$$

$$\begin{aligned}
& + \frac{-3+4\nu}{4\pi(-1+\nu)} \left\{ \left((-1/4 x_2 + 1/4 m_2) a_3^3 - 3/4 (x_3 + 1/3 m_3) a_2 a_3^2 \right. \right. \\
& \quad \left. \left. - 1/4 a_2^2 (-x_2 + m_2) a_3 - 1/4 a_2^3 (x_3 - m_3) \right) \right. \\
& \quad \cdot \ln \left[t^2 + ((2 m_2 - 2 x_2) a_2 + 2 a_3 (x_3 + m_3)) t + (x_2 - m_2)^2 + (x_3 - m_3)^2 \right] \\
& \quad + \left((a_3^2 x_3 + (-x_2 + m_2) a_2 a_3 - a_2^2 m_3) \right. \\
& \quad \left. \cdot \arctan \left[\frac{t a_2^2 + (-x_2 + m_2) a_2 + a_3 (x_3 + m_3 + a_3 t)}{(x_3 + m_3) a_2 - a_3 (-x_2 + m_2)} \right] + 1/2 a_2 t \right) a_3 \left. \right\} \\
& - \frac{1}{4\pi(-1+\nu)} x_3 \left\{ a_2 \left(a_3^2 t^2 + 2 t (x_3 + m_3) a_3 + a_2^2 t^2 + 2 t (-x_2 + m_2) a_2 \right. \right. \\
& \quad \left. \left. + m_3^2 + 2 x_3 m_3 + x_3^2 + (-x_2 + m_2)^2 \right) a_3^2 \right. \\
& \quad \cdot \ln \left[t^2 + ((2 m_2 - 2 x_2) a_2 + 2 a_3 (x_3 + m_3)) t + (x_2 - m_2)^2 + (x_3 + m_3)^2 \right] \\
& \quad + a_3 (a_2 - a_3) (a_2 + a_3) \left(a_3^2 t^2 + 2 t (x_3 + m_3) a_3 + a_2^2 t^2 \right. \\
& \quad \left. + 2 t (-x_2 + m_2) a_2 + m_3^2 + 2 x_3 m_3 + x_3^2 + (-x_2 + m_2)^2 \right) \\
& \quad \cdot \arctan \left[\frac{t a_2^2 + (-x_2 + m_2) a_2 + a_3 (x_3 + m_3 + a_3 t)}{(x_3 + m_3) a_2 - a_3 (-x_2 + m_2)} \right] \\
& \quad - t (-x_2 + m_2) a_3^4 + (3 t (x_3 + 1/3 m_3) a_2 - m_3 (-x_2 + m_2)) a_3^3 \\
& \quad + 2 a_2 \left(3/2 t (-x_2 + m_2) a_2 + 1/2 m_3^2 + 3/2 x_3 m_3 + x_3^2 + (-x_2 + m_2)^2 \right) a_3^2 \\
& \quad \left. - a_2^2 (t (3 m_3 + x_3) a_2 + m_3 (-x_2 + m_2)) a_3 - m_3 a_2^3 (x_3 + m_3) \right\} \\
& \quad \left/ \left((x_3 + m_3 + a_3 t)^2 + (x_2 - m_2 - a_2 t)^2 \right) \right.
\end{aligned}$$

And finally,

$$\begin{aligned}
I_{33}(t) = & - \frac{3-4\nu}{8\pi(1-\nu)} \left\{ \frac{1}{2} (t - (x_2 - m_2) a_2 - a_3 (x_3 - m_3)) \right. \\
& \quad \left. \cdot \ln \left[t^2 + ((2 m_2 - 2 x_2) a_2 + 2 a_3 (-x_3 + m_3)) t + (x_2 - m_2)^2 + (x_3 - m_3)^2 \right] \right. \\
& \quad \left. + ((x_3 - m_3) a_2 + a_3 (-x_2 + m_2)) \arctan \left[\frac{-t + (-m_2 + x_2) a_2 - a_3 (-x_3 + m_3)}{(-x_3 + m_3) a_2 - a_3 (-x_2 + m_2)} \right] \right\} \\
& + \frac{1}{8\pi(1-\nu)} \left\{ - a_3 a_2 ((x_3 - m_3) a_2 + a_3 (-x_2 + m_2)) \right.
\end{aligned}$$

$$\begin{aligned}
& \cdot \ln \left[t^2 + ((2m_2 - 2x_2)a_2 + 2a_3(-x_3 + m_3))t + (x_2 - m_2)^2 + (x_3 - m_3)^2 \right] \\
& + (a_2 - a_3)(a_2 + a_3)((x_3 - m_3)a_2 + a_3(-x_2 + m_2)) \\
& \cdot \arctan \left[\frac{-t + (-m_2 + x_2)a_2 - a_3(-x_3 + m_3)}{(-x_3 + m_3)a_2 - a_3(-x_2 + m_2)} \right] - ta_2^2 \left. \vphantom{\arctan} \right\} \\
& + \frac{8\nu^2 - 12\nu + 5}{8\pi(-1 + \nu)} \left\{ \frac{1}{2} (ta_2^2 + (m_2 - x_2)a_2 + a_3(x_3 + m_3 + a_3t)) \right. \\
& \cdot \ln \left[t^2 + ((2m_2 - 2x_2)a_2 + 2a_3(x_3 + m_3))t + (x_2 - m_2)^2 + (x_3 - m_3)^2 \right] \\
& + ((x_3 + m_3)a_2 - a_3(-x_2 + m_2)) \\
& \cdot \arctan \left[\frac{t + (-x_2 + m_2)a_2 + a_3(x_3 + m_3)}{(x_3 + m_3)a_2 - a_3(-x_2 + m_2)} \right] \left. \vphantom{\arctan} \right\} \\
& + \frac{1}{8\pi(-1 + \nu)} \left\{ 4a_3((x_3 + m_3)a_2 - a_3(-x_2 + m_2)) \right. \\
& \cdot ((x_3 + m_3)\nu - x_3 - 3/4m_3)a_2^2 - (-3/4 + \nu)a_3(-x_2 + m_2)a_2 - 1/4a_3^2x_3 \\
& \cdot \ln \left[t^2 + 2t((m_2 - x_2)a_2 + a_3(x_3 + m_3)) + (x_2 - m_2)^2 + (x_3 - m_3)^2 \right] \\
& + \left[-4 \left((m_2 + x_3 + m_3 - x_2)(-m_2 + x_3 + m_3 + x_2)\nu \right. \right. \\
& \quad \left. \left. - 5/4x_3^2 - x_3m_3 + 3/4(m_2 - m_3 - x_2)(m_2 + m_3 - x_2) \right) a_3^2 a_2^2 \right. \\
& \quad + \left(4(x_3 + m_3)^2\nu - 3m_3^2 - 8x_3m_3 - 3x_3^2 \right) a_2^4 \\
& \quad + a_3^3(8(x_3 + m_3)\nu - 6m_3 - 4x_3)(-x_2 + m_2)a_2 \\
& \quad - 8a_3(-x_2 + m_2)((x_3 + m_3)\nu - x_3 - 3/4m_3)a_2^3 \\
& \quad \left. + \left(-4(-x_2 + m_2)^2\nu + x_3^2 + 3(-x_2 + m_2)^2 \right) a_3^4 \right] \\
& \cdot \arctan \left[\frac{ta_2^2 + (-x_2 + m_2)a_2 + a_3(x_3 + m_3 + a_3t)}{(x_3 + m_3)a_2 - a_3(-x_2 + m_2)} \right] \\
& + (3 - 4\nu)t((x_3 + m_3)a_2 - a_3(-x_2 + m_2))a_2^2 \left. \vphantom{\arctan} \right\} \\
& \quad \left/ \left((x_3 + m_3)a_2 - a_3(-x_2 + m_2) \right) \right. \\
& + \frac{1}{8\pi(-1 + \nu)} \left\{ 4a_3((x_3 + m_3)a_2 - a_3(-x_2 + m_2)) \right. \\
& \cdot ((x_3 + m_3)\nu - x_3 - 3/4m_3)a_2^2 - (-3/4 + \nu)a_3(-x_2 + m_2)a_2 - 1/4a_3^2x_3 \\
& \cdot \ln \left(t^2 + 2((m_2 - x_2)a_2 + a_3(x_3 + m_3))t + (x_2 - m_2)^2 + (x_3 - m_3)^2 \right) \\
& \quad \left. + \left[\left(4(x_3 + m_3)^2\nu - 3m_3^2 - 8x_3m_3 - 3x_3^2 \right) a_2^4 \right. \right.
\end{aligned}$$

$$\begin{aligned}
& - 8 a_3 (-x_2 + m_2) ((x_3 + m_3) \nu - x_3 - 3/4 m_3) a_2^3 \\
& - 4 \left((m_2 + x_3 + m_3 - x_2) (-m_2 + x_3 + m_3 + x_2) \nu - 5/4 x_3^2 - x_3 m_3 \right. \\
& \quad \left. + 3/4 (m_2 - m_3 - x_2) (m_2 + m_3 - x_2) \right) a_3^2 a_2^2 \\
& + 8 a_3^3 ((x_3 + m_3) \nu - 3/4 m_3 - 1/2 x_3) (-x_2 + m_2) a_2 \\
& + 2 \left(-2 (-x_2 + m_2)^2 \nu + x_3^2 + 3/2 (-x_2 + m_2)^2 \right) a_3^4 \Big] \\
& \quad \cdot \arctan \left[\frac{t a_2^2 + (-x_2 + m_2) a_2 + a_3 (x_3 + m_3 + a_3 t)}{(x_3 + m_3) a_2 - a_3 (-x_2 + m_2)} \right] \\
& - 4 (-3/4 + \nu) t ((x_3 + m_3) a_2 - a_3 (-x_2 + m_2)) a_2^2 \Big\} \\
& \quad / \left((x_3 + m_3) a_2 - a_3 (-x_2 + m_2) \right).
\end{aligned}$$

The equations for I_{23} and I_{32} are numerically unstable in the limit $a_3 = 0$. For this special case, given that $\|\mathbf{a}\| = 1$, I take the analytical limit for $a_2 \rightarrow 1$ and $a_3 \rightarrow 0$. The codes to evaluate these equations, as well as any other solution presented in this manuscript, are available in an online repository (see the Data and Resources section).